IEEE Access
Multidisciplinary | Rapid Review | Open Access Journal

Received December 13, 2016, accepted January 3, 2017, date of publication January 16, 2017, date of current version June 7, 2017.

Digital Object Identifier 10.1109/ACCESS.2017.2649380

Delay and Throughput Analysis of Cognitive Go-Back-N HARQ in the Face of Imperfect Sensing

ATEEQ UR REHMAN[1], LIE-LIANG YANG[2], (Fellow, IEEE), AND LAJOS HANZO[2], (Fellow, IEEE)
[1]Department of Computer Science, Abdul Wali Khan University, Mardan 23200, Pakistan
[2]School of Electronics and Computer Science, University of Southampton, Southampton SO17 1BJ, U.K.

Corresponding author: Lajos Hanzo (lh@ecs.soton.ac.uk)

This work was supported in part by the EPSRC Project under Grant EP/Noo4558/1 and Grant EP/L018659/1, in part by the European Research Council Advanced Fellow Grant under the Beam-Me-Up Project, and in part by the Royal Society's Wolfson Research Merit Award.
This work was presented at the IEEE Vehicular Technology Conference, Nanjing, China, May 2016. The research data for this paper is available at http://doi.org/10.5258/SOTON/404271

ABSTRACT To mitigate spectrum scarcity, the cognitive radio (CR) paradigm has been invoked for improving the overall exploitation of the licensed spectrum by identifying and filling the free spectrum holes without degrading the transmission of primary users (PUs). Hence, we conceive a CR communication scheme, which enables a cognitive user (CU) to sense the activity of the PUs over a primary radio (PR) channel, which is exploited to transmit data using the modified Go-Back-N hybrid automatic repeat request (GBN-HARQ) protocol, when PR channel is free from the PUs. This arrangement is termed as the cognitive GBN-HARQ (CGBN-HARQ), whereby the activity of the PUs on the PR channel is modeled as a two-state Markov chain having "ON" and "OFF" states. However, the CU may wrongly detect the "ON"/"OFF" activity of the PUs in the channel, hence resulting in false-alarm or misdetection. Therefore, the two-state Markov chain is extended to four states by explicitly considering all the wrong sensing decisions. In this paper, we analytically modeled the CGBN-HARQ scheme with the aid of a discrete time markov chain (DTMC). Explicitly, an algorithm is developed for deriving all the legitimate states and for eliminating the illegitimate states, which assists us in reducing both the dimensionality of the state transition matrix and the associated computational complexity. Furthermore, based on DTMC modeling, we derive closed-form expressions for evaluating the throughput, the average packet delay, and the end-to-end packet delay of CGBN-HARQ in realistic imperfect sensing environment. The results are also validated by our simulations. Our performance results demonstrate that both the achievable throughput and the delay are significantly affected by the activity of the PUs as well as by the reliability of the PR channel and by the number of packets transmitted per time-slot (TS). To attain the maximum throughput and/or the minimum transmission delay, the number of packets transmitted within the TS should be carefully adapted based on the activity level of the PUs and on the quality of the PR channel.

INDEX TERMS ARQ, GBN-ARQ, primary radio, PR channel, cognitive radio, spectrum sensing, number of packets, cognitive GBN-HARQ, Discrete time Markov chain, throughput, delay.

LIST OF ACRONYMS

ACK	Positive Acknowledgement
ARQ	Automatic Repeat ReQuest
CGBN	Cognitive Go-Back-N
CR	Cognitive Radio
CSW	Cognitive Stop and Wait
CU	Cognitive User
DTMC	Discrete Time Markov Chain
DSA	Dynamic Spectrum Access
FEC	Forward Error Correction
GF	Galois Field
HARQ	Hybrid Automatic Repeat ReQuest
NACK	Negative Acknowledgement
OFF	Channel free from PU
ON	Channel occupied by PU
P_e	Packet Error Probability
PMF	Probability Mass Function
PR	Primary Radio
PU	Primary User
RS	Reed-Solomon
RTT	Round-Trip Time
SW	Stop and Wait
TS	Time-slot

LIST OF SYMBOLS

α	Probability of traversing from 'ON' to 'OFF' state
β	Probability of traversing from 'OFF' to 'ON' state
$\boldsymbol{I}$	Identity matrix
k	time duration used for sensing a TS
K_d	Information Bits of the codeword
L_i	Total number of new packets transmitted in state S_i
M_c	Total number of packets
M_T	Maximum delay
N	Number of packets in a TS
N_d	Coded symbols
$n_p(S_i)$	Function for storing number of new packets associated with state S_i
$\boldsymbol{P}$	Transition matrix
$\boldsymbol{p}$	Stores probabilities of all state in a TS
$\boldsymbol{P}_d$	Distribution of end-to-end delay packet delay by simulation
$P_{i,j}$	$\{i, j\}$th element of the transition matrix
P_{MF}	Distribution of end-to-end packet delay by analysis
P_{off}	Channel free probability
P_{on}	Channel busy probability
$\boldsymbol{\Phi}$	Steady-state vector
Φ_i	ith element of the Steady-state vector
$\boldsymbol{\pi}$	steady-state vector
π_i	ith element of steady-state vector
R_T	Throughput by analysis
R'_T	Normalized throughput by analysis
R_S	Throughput by simulation
$\mathbb{S}$	Sample set
S_i	Represents state i
$\mathbb{S}_N$	a set of states containing new packets
$\mathbb{S}_i$	Subset of $\mathbb{S}_N$, which contains states associated with new packet
$[\,]^T$	Represents matrix transpose
T	Total duration of the time-slot
T_d	duration for data transmission in a TS
T_D	Theoretically derived Total average packet delay
T'_{DS}	Total average packet delay obtained by simulation
T_p	Time duration for packet delivery
T_s	during for sensing a TS
τ	Theoretically derived Average end-to-end packet delay
τ_s	Average end-to-end packet delay obtained by simulation

I. INTRODUCTION

Since the germination of the cognitive radio concept [1], it has been considered to be one of the favourable regimes for mitigating the spectrum shortage that resulted from the inefficient spectrum utilization. The studies in [2]–[5] show that the inefficient utilization stems from the classic static spectrum allocation policy. Based on this policy, a certain bandwidth is exclusively allocated to a network, which is only available for the primary users (PUs). By contrast, CR relies on dynamic spectrum access (DSA), which allows both the PUs and CUs to share the licensed spectrum. For example, the CUs can sense and exploit the earmarked, but momentarily unoccupied licensed spectrum, which is referred to as a spectrum hole, and utilize it for their own transmissions [6]–[10]. However, the CUs have to evacuate the spectrum as soon as the PUs are reclaiming it. These capabilities of CR have encouraged the regulatory bodies to officially allow the deployment of CR systems in order to maximize the overall spectrum exploitation without having to make any changes to the existing PR systems operated under the classic fixed spectrum allocation approach [2], [10], [11]. As a result, various IEEE standards have incorporated the CR concept, including IEEE 1900, 802.11y, 802.16h, 802.22, etc., as shown in [12] and the references in it.

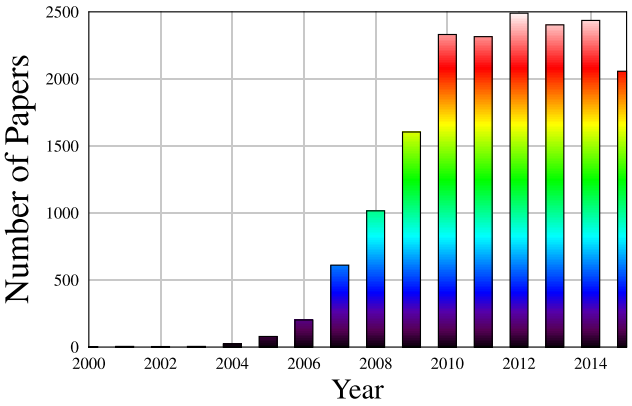

FIGURE 1. Number of contributions performed in the context of CR per year as per IEEE Xplore database.

In recent years, CR has attracted substantial research attention and has been systematically studied from diverse perspectives, as evidenced by the number of contributions dedicated to it, as shown in Fig. 1 [6]–[9], [13], [14]. Specifically, Haykin [8] has outlined the fundamental operating principles of CR systems in the context of spectrum sensing, channel estimation, cooperative communications, power control and dynamic spectrum management. In [6], [7], [9], the authors have addressed the spectrum sensing and resource allocation problems of CR. The architecture of the CR network and its impact on dynamic resource allocation have been studied in [13]. By contrast, Tragos *et al.* [14] have investigated the resource allocation techniques of both centralized and distributed CR networks, while considering the factors of interference, power, delay, etc. In CR, in addition to the challenges imposed by both spectrum sensing and DSA, CR systems also face the extra challenges, when aiming for a low BER. Therefore, powerful error-control approaches are required for achieving reliable communications, similarly to the traditional wireless communication systems [15], [16]. Some of the challenges associated with achieving reliable communication in CR systems are presented in the Fig. 2.

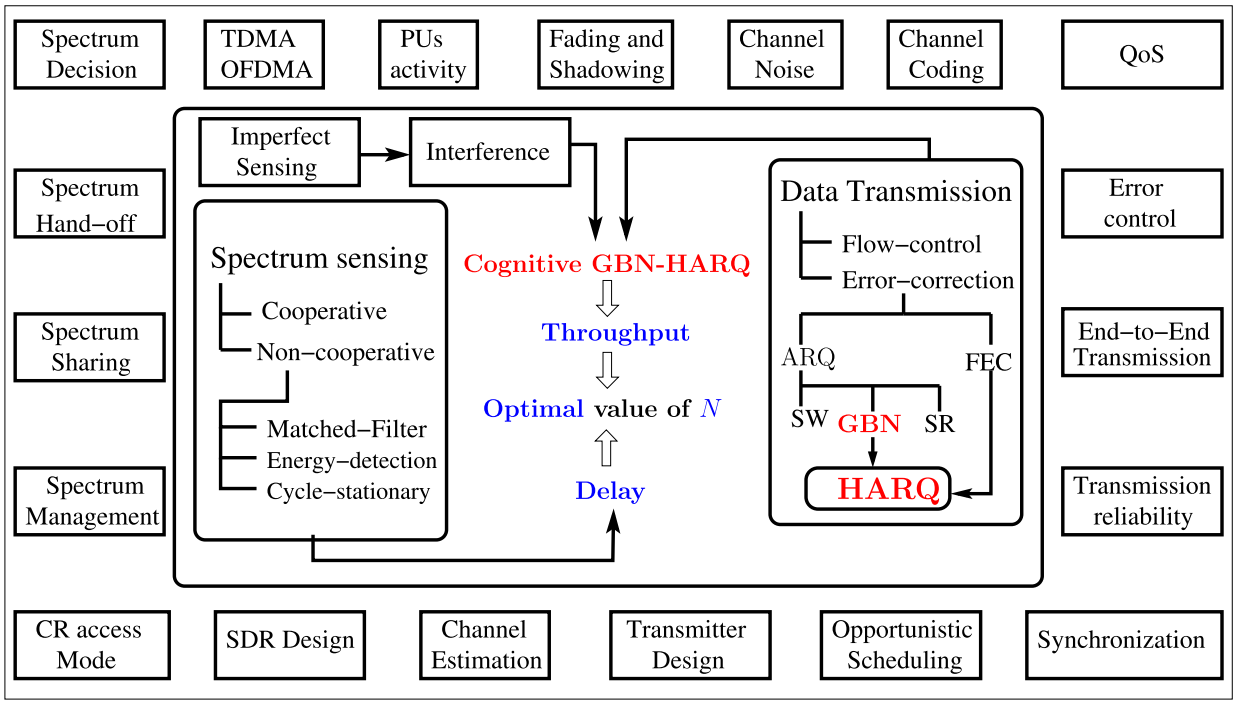

FIGURE 2. Overview of factors affecting the data transmission in CR systems.

Similar to previous studied [17]–[21] and [22]–[26], the activity of the PUs is modelled using a Markov chain having the 'ON' and 'OFF' states. Specifically, in the 'ON' state, the PR channel is considered to be occupied by the PUs, whereas in the 'OFF' state, it is free from PUs. In order to determine the status of the PR channel, the CR system invokes spectrum sensing and then accesses the channel, but only when it is deemed to be in the 'OFF' state. In practice, the sensing operation can never be perfect, therefore, the CR system may erroneously identify the PR channel's state, hence generating either a false-alarm or a mis-detection event. In this case, the channel perceived by the CR system may be described by a four state Markov chain by considering both the actual states of the PR channel and the states obtained after the sensing operation. Moreover, similar to [27]–[29], the PR's channel is organized in time-slots (TSs), where each TS has a duration of T seconds, which is divided into two sections of T_s and T_d seconds [27], [29]. The first T_s seconds of a TS are used for sensing the channel, while the remaining T_d seconds are utilized for data transmission, which follows the Go-Back-N hybrid automatic repeat request (GBN-HARQ) principles [15], [19], [20], [30], provided that the PR channel is deemed to be in the 'OFF' state.

In this paper, we specifically extend the classic GBN-HARQ protocol to the CR system, when imperfect sensing is considered. Here the GBN protocol has been favoured over other ARQ schemes, because its performance is better than that of the classic stop-and-wait HARQ (SW-HARQ), while its complexity is lower than that of the classic selective-repeat HARQ (SR-HARQ). Hence, we are interested in the characteristics and performance of the GBN-HARQ operated in CR communication environments, which is hence referred to as CGBN-HARQ. As mentioned above, in our CGBN-HARQ scheme, first the CR transmitter senses the status of the PR channel. If it is sensed to be free from the PUs, it transmits a number of packets based on the GBN-HARQ protocol. The CR receiver detects the packets one after another. Then the corresponding feedback is generated for each packet and fed back to the transmitter. When the transmitter receives a feedback, it (re)transmit the packets based on the feedback signal. Particularly, after each ACK flag, the transmitter sends a new packet, whereas for each NACK flag, the erroneous packet and all the subsequent packets are retransmitted in the next free TS.

This paper further develops our research on cognitive HARQ [17]–[21]. In a nutshell, in [17], [20], [21] we have studied both the throughput and delay of cognitive SW-HARQ (CSW-HARQ), cognitive Go-Back-N HARQ (CGBN-HARQ) and that of cognitive SR-HARQ (CSR-HARQ), all under the assumption of perfect spectrum sensing. By contrast, in [18], [19], we have characterized the throughput and delay of the CSW-HARQ and CGBN-HARQ schemes both for perfect and imperfect sensing. In more detail, in [18], we have conceived the throughput and delay of the CSW-HARQ scheme. On the other hand, in [19], we have investigated the performance of a CGBN-HARQ scheme in terms of its achievable throughput and delay. We assumed that the feedback flags are always received after the sensing duration of a TS, hence resulting in a simplified operational

model for analysing the CR transmitter, but at the cost of a longer round-trip delay and increased number of packet retransmissions. By contrast, in this paper, we relinquished the above constraint by enabling the transmitter to receive feedback flags any time during a TS (namely both during sensing as well as in the transmission epoch). Since the feedback information is well-protected and typically relies on a single-bit information [31], [32], the feedback overhead does not affect the sensing process and the PU's communication. By eliminating the above simplifying assumptions, the analytical modelling of the CGBN-HARQ scheme associated with imperfect sensing became challenging, due to: 1) the reception of the feedback flags both with in the sensing duration and data transmission duration; 2) the imperfect sensing decisions seen in our four-state Markov chain. By doing so, the transmitter circumvents the retransmission of packets for which ACK flags are received in the sensing period. As a result, both the overall throughput and the delay of the system are enhanced. Moreover, in contrast to [19], [20], in this treaties, the CGBN-HARQ is modelled by a DTMC, based on which closed-form expressions are derived both for the throughput as well as for the average packet delay and for the end-to-end packet delay. Our performance studies show that for achieving an increased throughput and a reduced delay, the number of packet transmission per TS requires a careful consideration for the sake of maximizing both the utility of PR channel and of the CR aided data transmission.

A. RELATED WORK

The performance of the classical ARQ protocols has been extensively characterized [15], [30], [58]. Specifically, the conventional GBN-ARQ has been modelled with the aid of DTMC and its throughput and delay was investigated in [59]–[66]. In more detail, Turin as well as Ausavapattanakun and Nosratinia [61], [64] invoked hidden Markov modelling and studied the throughput of GBN-ARQ, when considering both perfectly reliable and practically unreliable feedback in fading environments. In [62], Chakraborty and Liinaharja introduced an adaptive GBN-ARQ scheme operating in a time-varying fading channel and characterized its throughput. In this adaptive GBN-ARQ, the transmitter switches its transmission mode based on the reception of contiguous ACK's and NACK's. Moreover, Hayashida and Komatsu [59] as well as Zorzi and Rao [60] have studied the delay of the classic GBN-ARQ regime. As further advances, Zorzi [63] has designed block-coded error-control scheme operating under delay constraints and studied its performance. Qin and Yang [67]–[70] invoked ARQ techniques for a butterfly network topology and analyzed both its throughput as well as the probability mass function of its delay and its average packet delay. Similarly, Chen *et al.* proposed an algorithm based on Markov modelling for characterizing both the probability distribution and the average packet delay [65]. Li *et al.* proposed a cooperative GBN-HARQ scheme relying on a limited number of retransmissions [71]. The HARQ technique constitutes a promising design for achieving reliable communication, therefore it has been widely employed in wireless systems, as seen in the Timeline 1.

In the context of ARQ aided CR systems, there are only a limited number of references [79], [80], [93]–[103], which are illustrated in Timeline 2. However, none these references have provided the detailed theoretical throughput and delay analysis of ARQ-assisted CR systems. Specifically, in [93]–[95], it is assumed that the CUs infer the activity of the PUs via observing their feedbacks flags. Touati *et al.* [96] have performed the seminal performance analysis of ARQ-aided and relay-assisted CR systems. Yue *et al.* [97], [98] have proposed an improved HARQ scheme for the family of CR systems by invoking anti-jamming coding for achieving reliable communication. Furthermore, Liang *et al.* and Hu *et al.* [99], [100] studied the combination of spectrum interweave and underlay sharing access modes for the sake of maximizing the performance of the CUs. Specifically, Hu *et al.* [100] proposed ARQ techniques for maximizing the transmission reliability. On the other hand, in [101]–[103] comprehensive surveys have been presented for various communication techniques employed in CR systems.

However, to the best of the our knowledge, no published treaties has theoretically analyzed the delay and throughput of ARQ protocols in context of CR systems. The dynamic activities of PUs and the unreliable nature of spectrum sensing make the modelling and analysis of the ARQ protocols in CR systems challenging. Therefore, our objective is to model the family of HARQ-aided CR systems by deriving closed-form expressions for the throughput and delay of CGBN-HARQ schemes when imperfect spectrum sensing is assumed.

B. CONTRIBUTIONS AND PAPER STRUCTURE

Against the above background, the contributions of this paper are summarized as follows,

(a) *The cognitive protocol proposed in [20] is extended by enabling the transmitter to simultaneously sense and receive the feedback flag of the packet transmitted in the previous free TS in a realistic imperfect sensing environment. To do so, the CR transmitter requires significant improvements for reformulating the transmission principles of the classic GBN-HARQ, when incorporating it in CR systems.*

(b) *In contrast to [19], in this paper, the CGBN-HARQ has been theoretically modelled and analysed by a DTMC-based approach in imperfect sensing environments. Based on this model, closed form expressions are derived for the throughput, average packet delay and end-to-end packet delay. For the case of end-to-end packet delay, both its probability distribution and average end-to-end packet delay are analysed*

(c) *Finally, the theoretical analysis has been verified by the simulations.*

The rest of this paper is organized as follows. In Section II, we model the primary radio systems as well as the

TIMELINE 1: *Milestones of the conventional HARQ-aided wireless systems.*

1975 – The family of ARQ techniques was studied in satellite communications [33].
1984 – ARQ and HARQ techniques were studied by Lin *et al.* [34].
1988 – De *et al.* studied the performance of Type-II HARQ techniques [35].
1990 – Kallel introduced the code combining technique [36].
1994 – Decker investigated the family of HARQ techniques in GSM [37].
1997 – Zorzi *et al.* characterized the ARQ regimes in fading mobile radio channels [38].
1999 – Hamorsky and Hanzo studied the performance of turbo coded Type-II HARQ [39].
2000 – Sozer *et al.* characterized various ARQ paradigms in underwater acoustic networks [40].
2001 – Caire and Tuninetti investigated the performance HARQ in Gaussian fading channels [41].
2003 – Kim *et al.* quantified the performance of HARQ protocols in mobile communication [42].
2005 – Zhao and Valenti studied *ad hoc* networks, when HARQ was employed [43].
2007 – Beh *et. al* investigated the HARQ techniques of LTE OFDMA systems [44].
2009 – Vuran and Akyildiz provided the cross-layer analysis of error control techniques [45].
2010 – Zhang and Hanzo proposed HARQ aided superposition coding [46], [47].
2011 – Chen *et al.* introduced multi-component turbo coded HARQ techniques [48]–[50].
2013 – Chen *et al.* discussed the challenges of concatenating HARQ and turbo codes [51], [52].
2014 – Ngo and Hanzo presented the state-of-the-art of HARQ techniques in cooperative communications [53].
2015 – Chen *et al.* introduced an adaptive HARQ scheme by amalgamating Raptor codes and HARQ [54].
2015 – Xu *et al.* proposed Type-III HARQ based on network coding and distributed turbo coding [55].
2016 – Zhu *et al* introduced truncated HARQ technique for reducing the video distortion [56].
2016 – Makki *et al.* characterized the performance of HARQ-aided and relay assisted networks [57].

TIMELINE 1. Milestones of the conventional HARQ-aided wireless systems.

cognitive systems. In Section III, we outlined the transmission principles of CGBN-HARQ, whereas the operation of the CR transmitter and receiver is presented in Subsections III-A and III-B, respectively. Then, we detailed our DTMC-based analytical model in Section IV. Then, closed-form expressions are derived for the throughput and delay in the Subsections IV-D and IV-E, which are then verified by our simulations presented in Section V. Finally, the conclusions of this contribution are provided in Section VI.

II. SYSTEM MODEL

In this section, we will model both the PR and CR systems. Furthermore, the main assumptions used are described.

A. MODELLING OF PRIMARY RADIO SYSTEMS

Similar to our previous studies [19], [20], a two-state Markov chain having 'ON' and 'OFF' states is invoked for modelling the activities of PUs in the PR channel, as shown in Fig. 3. In the 'ON' state, a PU is assumed to be utilizing the PR channel, while in the 'OFF' state, the PR channel is free from the PUs. The transition probability from the 'OFF' to the 'ON' and that from 'ON' to 'OFF' state are represented by β and α, respectively. Let P_{on} and $P_{off} = 1 - P_{on}$ represent the probabilities of the PR channel being in the 'ON' and 'OFF' states. Then, when the Markov chain reaches its steady state, we have [30]

$$P_{on}\alpha = P_{off}\beta, \tag{1}$$

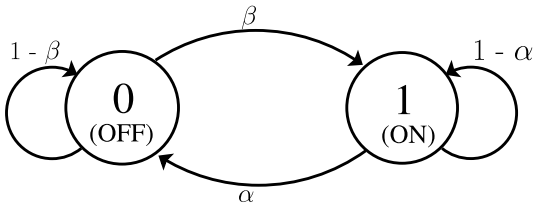

FIGURE 3. Two-state discrete-time Markov chain model for PR systems [23]–[25].

TIMELINE 2: *Milestones in CR-aided HARQ systems.*

- 2001 – Ramos and Madani studied software defined radio systems, especially their protocol layer [72].
- 2005 – Cabric and Brodersen introduced a transmission scheme based on wide-band power control and spectrum shaping [73].
- 2006 – Fujii *et al.* focused on space-time-block-coding assisted distributed ARQ in *ad hoc* CR networks [74].
- 2006 – Devroye *et. al* investigated the communication limits of CR systems [75].
- 2007 – Weingart *et. al* investigated the parameters of the physical-network-and-application-layer for the sake of improving both the spectrum efficiency and reliability [76].
- 2008 – Cheng and Zhen combined power controlled modulation with truncated ARQ for improving the overall throughput of CR systems [77].
- 2009 – Yue and Wang introduced an anti-jamming coding technique in the context of CR systems for improving the reliability [78].
- 2010 – Ao and Chen introduced HARQ assisted amplify-and-forward cooperative relaying into CR systems [79].
- 2010 – Yang *et al.* invoked network coding for CR systems for improving the efficiency of classic ARQ techniques [80].
- 2011 – Cheng *et al.* focussed their attention on improving the data rate of CR system by observing the ARQ feedback flags of PUs [81].
- 2012 – Makki *et al.* characterized the throughput and outage probability of CR aided HARQ systems [82].
- 2013 – Andreotti *et al.* introduced a link adaptation paradigm for increasing the goodput, whilst reducing the complexity [83].
- 2014 – Ozcan *et al.* characterized the error rate performance of CR systems [84].
- 2014 – Chen *et al.* focused their efforts on the end-to-end transmission improvements of CR-aided *ad hoc* networks [85].
- 2015 – Zou *et al* proposed an opportunistic relay assisted scheme for improving the reliability of CR systems [86].
- 2015 – Makki *et al.* invoked finite-length codewords in spectrum sharing CR networks and studied their throughput [87], [88].
- 2016 – Khan *et al.* reviewed the networking techniques, applications and CR communication protocols employed in smart grids [89].
- 2016 – Zhang *et. al* introduced energy-efficient DSA protocols for improving the overall channel utilization without degrading the PUs performance [90].
- 2016 – Patel *et al.* focused on maximizing the achievable rates of CR systems [91], [92].

TIMELINE 2. Milestones in CR-aided HARQ systems.

which results in

$$P_{on} = \frac{\beta}{\alpha + \beta}, \quad P_{off} = \frac{\alpha}{\alpha + \beta}. \tag{2}$$

Similar to our previous contributions [18]–[20] and as shown in Fig. 4(a), the PUs utilize the channel on the basis of TSs, whereas the activation of each TS is independent and has the same probability. Similarly, we also assume that when a TS is found in the 'OFF' or 'ON' state, the PUs activity remains the same until the end of that TS. For instance, when a TS is deemed to be in the 'OFF' state, the CU is allowed to access the TS and send its own data. Otherwise, the CU waits until the next TS [22].

B. MODELLING OF COGNITIVE SYSTEMS

In CR systems, each TS is further partitioned into the sensing time duration of T_s seconds and data transmission in the remaining of $T_d = T - T_s$ seconds, as presented in Fig. 4(b). As mentioned above, in the sensing duration, the CUs perform sensing for the sake of determining the 'ON' and 'OFF' activity of the PUs in the channel considered. If the PR channel is deemed to be free, then in the remaining

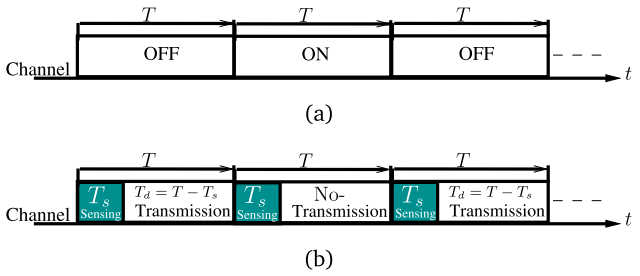

FIGURE 4. Time-slot structure of PR and CR systems, where a CR TS consists of a sensing duration of T_s and a transmission duration of $T_d = T - T_s$, when given the total duration T of a time-slot. (a) Channel utilization by PU. (b) Channel Utilization by CU.

T_d seconds the CU embarks on data transmission using the classic GBN-HARQ protocol, which will be detailed below. Otherwise, it waits until the next TS, during which the above procedure is repeated.

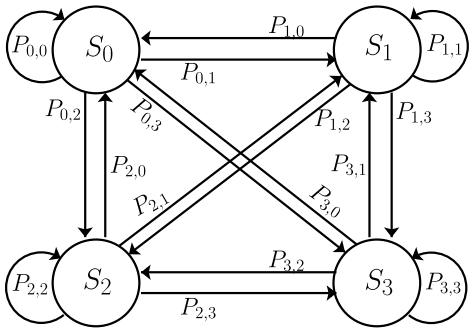

FIGURE 5. Modelling the CR system in the face of realistic imperfect sensing with the help of a four-state Markov chain, where $S_0 = 00$ represents the case in which the TS is free in reality, and the CU correctly sensed it as being free. $S_1 = 01$ illustrates that the channel is free in reality, but the CU detected it to be busy. Likewise $S_2 = 10$ and $S_3 = 11$.

It is widely recognized that the sensing operation cannot be perfectly reliable in practice, hence there is always a chance of incorrect sensing, due to numerous problems, such as for example the channel-induced shadowing and fading, aggravated by the background noise. Similarly, in the context of CR systems, it may also wrongly detect the presence/absence of PUs in the PR channel, hence resulting either in false-alarm (P_{fa}) or in mis-detection (P_{md}). To elaborate a little further, false-alarm represents the scenario, in which the PU is inactive but the CR system deems it to be active. On the other hand, mis-detection represents the case, in which the PU is active, yet the CR system deemed the channel to be free. In summary, the states of this realistic CR system are shown in Fig. 5, where the index of each state is the combination of a two-digit sequence, where the first digit illustrates the real status of the PR channel, whereas the second digit represents the sensed status of the channel. Additionally, the transition probability between states can be readily arranged in a matrix form as

$$\boldsymbol{P} = \begin{bmatrix} P_{0,0} & P_{0,1} & P_{0,2} & P_{0,3} \\ P_{1,0} & P_{1,1} & P_{1,2} & P_{1,3} \\ P_{2,0} & P_{2,1} & P_{2,2} & P_{2,3} \\ P_{3,0} & P_{3,1} & P_{3,2} & P_{3,3} \end{bmatrix}.$$

Then, with the aid of (2) and Fig. 5, we obtain

$$\begin{aligned} P_{0,0} &= P_{1,0} = (1-\beta)(1-P_{fa}) \\ P_{0,1} &= P_{1,1} = (1-\beta)P_{fa} \\ P_{0,2} &= P_{1,2} = \beta P_{md} \\ P_{0,3} &= P_{1,3} = \beta(1-P_{md}) \\ P_{2,0} &= P_{3,0} = \alpha(1-P_{fa}) \\ P_{2,1} &= P_{3,1} = \alpha(1-P_{fa}) \\ P_{2,2} &= P_{3,2} = (1-\alpha)(P_{md}) \\ P_{2,3} &= P_{3,3} = (1-\alpha)(1-P_{md}). \end{aligned} \tag{3}$$

Let us express the steady-state probabilities of the Markov chain as $\boldsymbol{\Phi} = [\Phi_0, \Phi_1, \Phi_2, \Phi_3]^T$. Then, we have

$$\boldsymbol{\Phi} = \boldsymbol{P}^T \boldsymbol{\Phi}, \tag{4}$$

which demonstrates that $\boldsymbol{\Phi}$ is the right eigenvector of $\mathbf{P}^T$ having an eigenvalue of one. Therefore, based on (4), we have

$$\begin{aligned} \boldsymbol{\Phi} &= [\Phi_0 \;\; \Phi_1 \;\; \Phi_2 \;\; \Phi_3]^T \\ &= \lambda \times \left[\frac{\alpha(1-P_{Fa})}{\beta(1-P_{md})} \;\; \frac{\alpha(P_{Fa})}{\beta(1-P_{md})} \;\; \frac{(P_{md})}{(1-P_{md})} \;\; 1 \right]^T, \end{aligned} \tag{5}$$

where $\lambda \in \mathbb{R}$ is applied to satisfy

$$\sum_{i=0}^{3} \Phi_i = 1, \tag{6}$$

giving

$$\lambda = \frac{\beta(1-P_{md})}{\alpha+\beta}. \tag{7}$$

Upon substituting (7) into (5), the steady-state probabilities of the CR system at states S_0, S_1, S_2 and S_3 are given by

$$\Phi_0 = \frac{\alpha(1-P_{fa})}{\alpha+\beta}, \quad \Phi_1 = \frac{\alpha(P_{fa})}{\alpha+\beta} \tag{8}$$

$$\Phi_2 = \frac{\beta(P_{md})}{\alpha+\beta}, \quad \Phi_3 = \frac{\beta(1-P_{md})}{\alpha+\beta}. \tag{9}$$

III. PRINCIPLES OF COGNITIVE GO-BACK-N HYBRID AUTOMATIC REPEAT REQUEST

Similar to our previous studies [19], [20], in this treatise, the CR system also transmits its data in the form of packets, where each packet is assumed to be encoded by Reed-Solomon (RS) codes defined over the Galois Field of GF(q)=GF(2^m). Each RS coded packet is comprised of N_d and K_d symbols. Specifically, N_d represents the information symbols, whereas K_d denotes the coded symbols. Moreover, we assumed that each RS coded packet requires a duration of T_p seconds for its transmission. As a result, the transmitter is capable of sending $N = T_d/T_p$ packets in each free TS. Furthermore, we also assumed that the RS code is capable of perfectly detecting and rectifying t errors. However, when more than t symbol errors are received in a packet, it discards the packet.

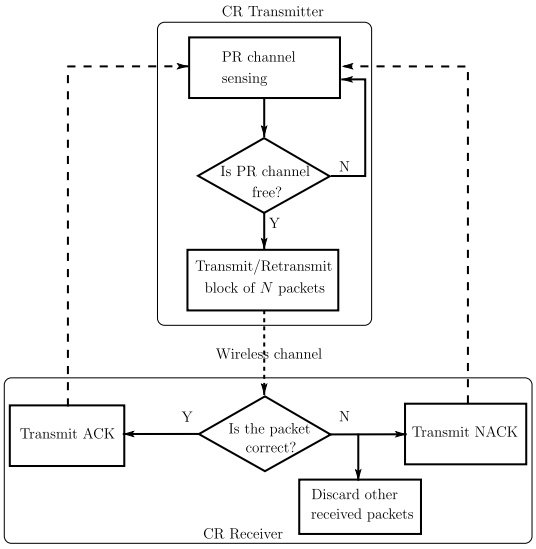

FIGURE 6. Flow chart showing the operations of the proposed CGBN-HARQ scheme.

Following the above assumptions and as illustrated in Fig. 6, the data packets are transmitted between a pair of CR users, namely the CR transmitter and CR receiver, while relying on the principles of the CGBN-HARQ scheme. Similar to the classic GBN-HARQ [15], [30], [58], the CR transmitter seamlessly transmits N packets one after another in a free TS, without waiting for their feedback flags, where the feedback for each packet is programmed to be received after the round-trip-time (RTT) of T_d seconds. The RTT can be defined as the time duration spanning from the commencement of packet transmission until the reception of its feedback flag [15], [30], [58]. Note that during the RTT of a packet, the subsequent $(N-1)$ packets are also transmitted.

Below we provide more details concerning the operational principles of the CGBN-HARQ based CR transmitter and CR receiver, which was described by Algorithm 1 of [20] in a perfect sensing scenario. By contrast, the additional consequences imposed by imperfect sensing are discussed as follows.

- When a TS is mis-classified, the transmitter sends N packets to the receiver following the normal procedure described in Algorithm 1 of [20].
- In the case of false-alarm, even though the channel is free, the CR transmitter does not transmit packets.
- At the receiver side, in the mis-detection scenario, the receiver discards the packet with a probability of one, since the probability of the packet being in error is too high both due to its collision with the PUs transmission and the channel noise.

A. OPERATION OF THE CR TRANSMITTER

In the conventional GBN-HARQ protocol, the packets are continuously transmitted by the transmitter until it receives a negative feedback flag (NACK). In this case, the retransmission of the corrupted and of all subsequent packets has to take place. In the CGBN-HARQ scheme of this contribution, however, the PR channel is first sensed by the CR transmitter for T_s seconds. If the TS is detected to be free from PUs, the corresponding packets are transmitted, otherwise the transmitter waits for the next TS. Additionally, in realistic imperfect sensing environments the transmission of packets takes place, when the PR channel is correctly detected to be in the 'OFF' state, or when it is deemed to be in the 'OFF' state but it is actually 'ON'. On the other hand, if the PR channel is in the 'ON' state or falsely deemed to be in the 'ON' state, the transmitter waits for the next TS and repeats the process of sensing. In summary, in each free TS, the transmitter sends N packets. These packets may be either new or those that require retransmission.

Moreover, as in the classical GBN-ARQ, it assumed that the CR transmitter has a buffer size of N packets and it follows the first-in-first-out principle [15], [30], [58]. In the transmitter buffer the copies of the transmitted packets are stored until it receives a positive feedback (ACK) flag. For example, if an ACK is received for a packet, the CR transmitter removes its copy from the buffer and replaces it with a new packet. On the other hand, if a NACK flag is received, the transmitter buffer remains unchanged. Furthermore, it is assumed that the transmission of feedback flags is always error-free. This may be justified, since a single bit of feedback information is sufficient for the CGBN-HARQ, which can be strongly protected from errors [31], [32]. This justifies our assumption of allowing the CR transmitter to receive feedback flags at any time in a busy or free TS, without hampering the sensing process or the PU transmission, as shown in Figs. 7 and 8.

It is worth noting that when feedback flags are received during sensing time, the transmitter only updates its buffer and waits until the decision about the TS takes place. For instance, as shown in Fig. 7, the ACK flag for packet 1 is received during sensing time, hence the transmitter replaces the copy of packet 1 by packet 5 and waits for the sensing result. Soon after the sensing decision took place and ACK flags were received in the transmission period, the transmitter sends the new packets 5, 6, 7, 8 in the free TS, as illustrated in TS T_2 of Fig. 7. The process continues until a NACK flag is received, as shown in Fig. 8. The transmitter immediately stop sending new packets and prepares for retransmitting both the corrupted and the subsequent packets. Moreover, in the case of a busy TS, the transmitter prepares the sequence of packets in the buffer for transmitting them in the next free TS, as shown in TS T_3 and T_4 of Figs. 7 and 8.

It is worth noting that in Fig. 7, TS T_2 is mis-detected, which implies that the TS is actually occupied by the PU, but due to the wrong sensing decision, it is declared to be free. As a result, new packets, i.e., packets 5, 6, 7 and 8, of Fig. 7 are transmitted. However, due to their collisions with the PU transmissions, these packets are corrupted and hence all N packets are received in error. Moreover, in the case of false-alarm, the free TS is sensed to be busy, hence no transmission takes place.

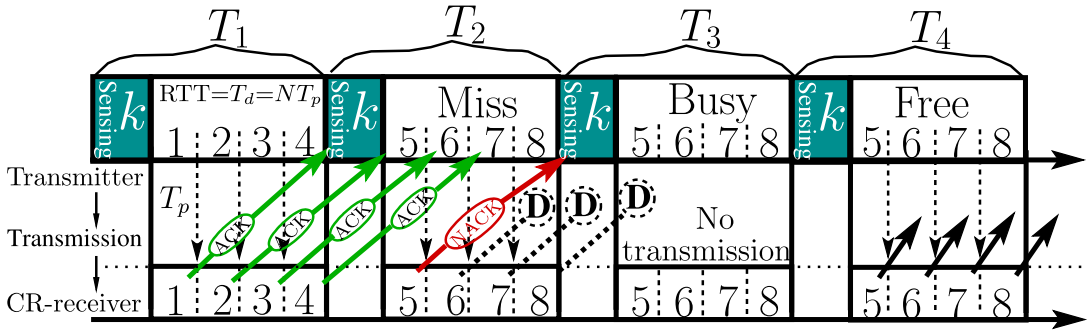

FIGURE 7. Packet transmission using the CGBN-HARQ scheme, when $k = 1$ and $N = 4$ in the case of imperfect sensing.

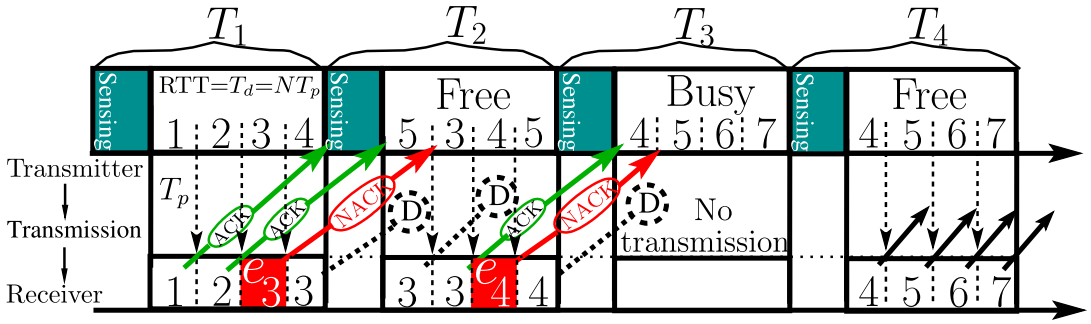

FIGURE 8. Packet transmission using the CGBN-HARQ scheme, when $k = 1$ and $N = 4$, illustrating the effect of the NACK flag in both free and busy TSs.

B. OPERATION OF THE CR RECEIVER

In this contribution, the CR receiver works in a similar way as that proposed in our previous studies [19], [20]. This is because, the receiver has no information about the sensing or the PU's activity in the channel. However, it only performs RS decoding of the received packets and generates the respective feedback flags, which are then sent to the transmitter. For example, as shown in Fig. 7 and 8, if a packet is declared to be error-free after error-correction, the receiver transmits an ACK flag to inform the transmitter that the packet is correctly received, hence a new packet is required. On the other hand, if the NACK flag is transmitted due to erroneous reception of a packet, the transmitter sends both the erroneous and the subsequent packets again. Moreover, in the case of mis-detection, the CR receiver considers the packet to be erroneous and feeds back a NACK flag to the transmitter's control channel receiver for the respective packet.

IV. DISCRETE TIME MARKOV CHAIN BASED ANALYSIS

In contrast to the classic GBN-HARQ protocol, the modelling of the CGBN-HARQ transmission scheme in imperfect sensing environments hinges on the dynamic activity of the PU and on the potentially incorrect sensing of the PR channel. In this paper, the CGBN-HARQ transmission scheme has been modelled by DTMC in a realistic imperfect sensing environment. Based on the DTMC modelling, we then evaluate the steady-state throughput, average packet delay and the end-to-end delay considering both its probability distribution and the average end-to-end packet delay.

To commence the analysis, the states of the CGBN-HARQ system can be jointly determined by the following factors:

(a) The actual status of the PR channel.
(b) The sensed status of the PR channel.
(c) The status of the N packets stored in the transmitter buffer, (which may be 'new', 'old' and 'packets transmitted twice in a TS').

Let us formulate the list of states as

$$\mathbb{S} = \{S_0, S_1, \ldots, S_i, \ldots S_T\}, \tag{10}$$

where S_T represents the total number of states, i.e we have $S_T = |\mathbb{S}|$, and S_i is the ith state in $\mathbb{S}$ and has an $(N+2)$-length base-3 digit formulated as

$$S_i = \{S_{i0}S_{i1}S_{i2}\cdots S_{i(N+1)}\}, \quad i = 0, 1, \cdots \tag{11}$$

For convenience, S_i represents the ith state sequence. Specifically, in the state sequence of Eq (11), the first digit S_{i0} illustrates the real status of the PR channel,

$$S_{i0} = \begin{cases} 0, & \text{if the PR channel is free in real,} \\ 1, & \text{if the PR channel is busy in real.} \end{cases} \tag{12}$$

The second digit S_{i1} represents the sensed status of the PR channel, which is given by

$$S_{i1} = \begin{cases} 0, & \text{if the PR channel is sensed free;} \\ 1, & \text{if the PR channel is sensed busy.} \end{cases} \quad (13)$$

Finally, the digit S_{ij} for $j = 2, \ldots, N+1$, is determined as

$$S_{ij} = \begin{cases} 0, \text{ if the } j\text{th packet is a new one;} \\ 1, \text{ if the } j\text{th packet is a retransmitted one,} \\ \quad \text{when the TS is free; or the one to be} \\ \quad \text{retransmitted, when the TS is busy;} \\ 2, \text{ if the } j\text{th packet is a repeated replica} \\ \quad \text{of a previous packet in the same TS.} \end{cases} \quad (14)$$

Having determined S_{ij} according to (12), (13) and (14), we can find a one-to-one mapping between i and S_i as

$$i = \sum_{j=0}^{N+1} S_{ij} 3^{N-j+1}, \quad (15)$$

which gives the subscript i of S_i, representing the ith state of the DTMC.

For the sake of deep understanding, a pair of examples are provided below, which explains the DTMC-based modelling in the face of imperfect sensing in terms of the associated state transitions.

TABLE 1. Possible states of the CGBN-HARQ, with $N = 1$ and $k = 1$.

State	$(S_{i0}$	S_{i1}	$S_{i2})$	State	$(S_{i0}$	S_{i1}	$S_{i2})$
S_0	(0	0	0)	S_9	(1	0	0)
S_1	(0	0	1)	S_{10}	(1	0	1)
S_3	(0	1	0)	S_{12}	(1	1	0)
S_4	(0	1	1)	S_{13}	(1	1	1)

A. EXAMPLE 1

Let us examine the CGBN-HARQ scheme using a single T_p for the sensing process, which is only capable of transmitting a single packet (i.e. $k = 1$ and $N = 1$). In other words, the transmitter buffer stores the copy of a single packet. In this scenario, a packet will never be repeated in the same TS and therefore digit 2 of Eq. (14) will never appear in the state sequence. According to the above definitions, we can show that the DTMC of this system has $S_T = 8$ states, which are explicitly shown in Table 1. Correspondingly, the state transitions are shown in Fig. 10, where the transitions and their transition probabilities are detailed below. Let us assume that the transmitter is initially in state $S_0 = 000$. This state is defined by the events that the TS is actually free (i.e. $S_{i0} = 0$) and it is also sensed to be free by the CR system (i.e. $S_{i1} = 0$). Therefore, the transmission of a new packet takes place ($S_{i2} = 0$). Moreover, when the transmitter receives an ACK flag related to the transmitted packet and the next TS is again correctly detected to be free, the transmitter remains in the same state S_0. This gives the transition probability of $P_{0,0} = P_{off}(1 - P_{fa}) \times (1 - P_e)$, where P_e is the packet's error probability. By contrast, if the transmitter receives a NACK flag and the TS is found to be free from PUs, the system traverses to state $S_1 = 001$. Correspondingly, the transition probability is $P_{0,1} = P_{off}(1 - P_{fa}) \times P_e$. In a similar manner, if the next TS is correctly detected to be busy and an ACK (or a NACK) flag is received, then the transmitter changes its state from S_0 to S_{12} (or S_{13}), with a transition probability of $P_{0,12} = P_{on}(1 - P_{md}) \times (1 - P_e)$ (or $P_{0,13} = P_{on}(1 - P_{md}) \times P_e$). Likewise, if the next busy TS is mis-detected and an ACK (or NACK) flag is received, then the transmitter traverses from S_0 to S_9 (or S_{10}), with a transition probability of $P_{0,9} = P_{on}P_{md} \times (1 - P_e)$ (or $P_{0,10} = P_{on}P_{md} \times P_e$).

When the transmitter is in state S_9 or S_{10}, in the next TS the transmitter can only make a transition to one of the following states S_1, S_4, S_{10} and S_{13}. This is because the transmissions associated S_9 and S_{10} are always assumed to be incorrect due to mis-detection. If the next TS yields false-alarm or it is correctly detected to be busy, then the transmitter moves to state S_4 or S_{13}, associated with the transition probability of $P_{9,4} = P_{off}P_{fa}$ or $P_{9,13} = P_{on}(1 - P_{md})$. Similarly, based on Fig. 10, the remaining state transitions can be readily analyzed, where in Table 2, we presented the corresponding state to state transition probabilities.

B. EXAMPLE 2

In the second example, we considered the CGBN-HARQ scheme having the parameters of $k = 1$ and $N = 4$. For clarity, we consider the scenario shown in Fig. 9, which illustrates that the transitions take place across five TSs, with the following justification.

(a) Let us consider in TS T_1 that the PR channel is correctly detected to be free. Hence, we have $S_{i0} = 0$ and $S_{i1} = 0$. In this case, we assume that $N = 4$ new packets are transmitted, which give $S_{ij} = 0$ for $j = 2, 3, 4, 5$. Therefore, at the end of TS T_1, the state observed by the transmitter is $S_0 = \{0, 0, 0, 0, 0, 0\}$. As shown in the figure, the first two packets are received without errors, therefore ACK flags are transmitted. By contrast, packet 3 is erroneously received, hence the receiver feeds back a NACK flag to the transmitter.

(b) Due to mis-detection, the TS T_2 is deemed to be free, although it is actually busy. Therefore, the transmitter receives an ACK after the sensing duration and it transmits the new packet 5. However, after the reception of a NACK flag at the end of the first T_p of the transmission duration of T_2, both the corrupted as well as the subsequent packets are retransmitted, where the indices of the 4 packets transmitted during T_2 are 5, 3, 4, 5. It is worth noting that packet 5 is transmitted twice in the same TS, while packets 3 and 4 are old packets transmitted in the previous TS, as depicted in Fig. 9. All the above-mentioned events result in the

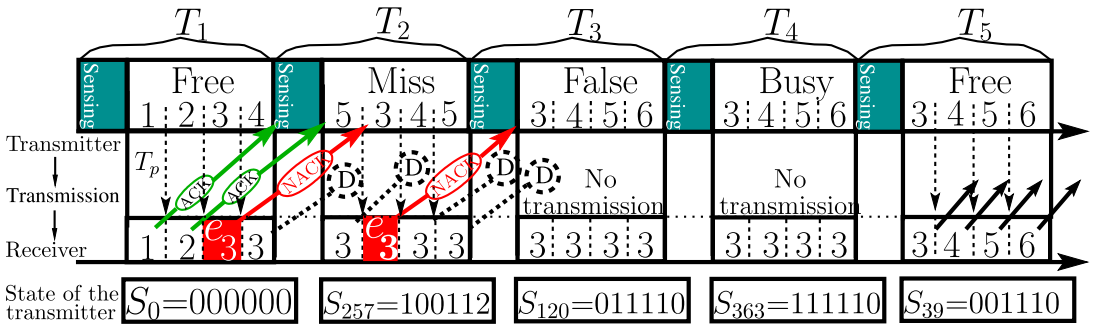

FIGURE 9. Packet transmission using CGBN-HARQ, where Miss and False represent misdetection and false-alarm, respectively. At the end of the TS, the transmitter state is observed.

TABLE 2. State-to-state transition probabilities with respect to TS for $N = 1$ and $k = 1$ case.

Current State S_i	State S_j probability	State S_j probability	State S_j probability	State S_j probability
$P_{i,j}$=$i = 0, 1$ & $j = 0, 1, 3, \ldots 13$	$P_{i,0}$=$P_{off}(1\text{-}P_{fa})(1\text{-}P_e)$ $P_{i,9}$=$P_{on}P_{md}(1\text{-}P_e)$	$P_{i,1}$=$P_{off}(1\text{-}P_{fa})P_e$ $P_{i,10}$=$P_{on}P_{md}P_e$	$P_{i,3}$=$P_{off}P_{fa}(1\text{-}P_e)$ $P_{i,12}$=$P_{on}(1\text{-}P_{md})(1\text{-}P_e)$	$P_{i,4}$=$P_{off}P_{fa}P_e$ $P_{i,13}$=$P_{on}(1\text{-}P_{md})P_e$
$P_{i,j}$=$i = 3, 12$ & $j = 0, 1, 3 \ldots 13$	$P_{i,0}$=$P_{off}(1\text{-}P_{fa})$ $P_{i,9}$=$P_{on}P_{md}$	$P_{i,1} = 0$ $P_{i,10} = 0$	$P_{i,3}$=$P_{off}P_{fa}$ $P_{i,12}$=$P_{on}(1\text{-}P_{md})$	$P_{i,4} = 0$ $P_{i,13} = 0$
$P_{i,j}$=$i = 4, 8, 9, 13$ & $j = 0, 1 \ldots 7$	$P_{i,0} = 0$ $P_{i,9} = 0$	$P_{i,1}$=$P_{off}(1\text{-}P_{fa})$ $P_{i,10}$=$P_{on}P_{md}$	$P_{i,3} = 0$ $P_{i,12} = 0$	$P_{i,4}$=$P_{off}P_{fa}$ $P_{i,13}$=$P_{on}(1\text{-}P_{md})$

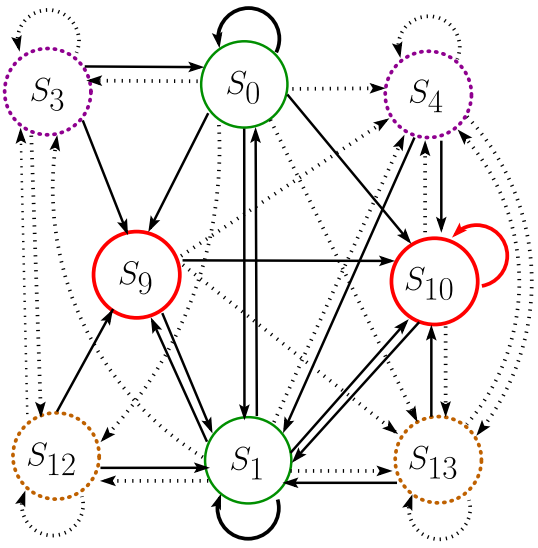

FIGURE 10. State diagram illustrating the modelling of the CGBN-HARQ scheme for $N = 1$ and $k = 1$. The *dashed* lines denote the transitions to the busy states only, due to the detection of a busy TS. On the other hand, *solid* lines represent the transitions to the free states during the detection of free TSs. The *solid* circles illustrate the free states as the result of correct detection and mis-detection, whereas *dashed* circles denote the busy states as the result of correct detection and false-alarm.

state associated with the index of $S_{257} = 100112$ in TS T_2. Correspondingly, the transition probability from state S_0 to S_{257} is $P_{0,257} = P_{on}P_{md} \times (1 - P_e)^2 P_e$. Moreover, since the TS T_2 is mis-detected, the packets transmitted in TS T_2 are all received in error. Hence, the receiver feeds back a NACK flag, while packets 4 and 5 are discarded, regardless whether they are received correctly or incorrectly.

(c) During TS T_3, the channel is falsely detected to be busy. Since all packets transmitted during the TS T_2 are erroneous, they require retransmission. Hence, the transmitter changes its state from S_{257} to $S_{120} = 011110$ with a probability of $P_{257,120} = P_{on} \times P_{md}$.

(d) Following the same pattern, the state associated with TS T_4 is S_{363} and the corresponding transition probability from state S_{120} to S_{363} is $P_{257,363} = P_{on} \times (1 - P_{md})$.

(e) Finally, the TS T_5 is correctly detected to be free. Therefore, all the N packets waiting in the buffer are transmitted, which results in a transition from state S_{363} to the state S_{39} with a transition probability of $P_{363,39} = P_{off} \times (1 - P_{fa})$.

According to the principles of our CGBN-HARQ, the characteristics of the DMTC derived for the CGBN-HARQ relying on realistic imperfect sensing are given below.

- In a busy TS, there will be no transmission or retransmission of a packet, therefore the respective state sequence does not contain digit 2. This busy state can be encountered either due to correct sensing of an occupied PR channel, or owing to the false-alarm encountered in a free PR channel.
- When a transition from a busy state to a free state occurs, only the first two digits of the current state sequence S_{i0} and S_{i1} may change in the new state sequence. This is explicitly shown in TS T_5 of Fig. 9. Hence, digit 2 does not appear in the new state sequence.
- The first two digits of a state sequence, i.e. S_{i0} and S_{i1}, never assume a value of 2.

With the aid of these properties, large fractions of the states can be eliminated from consideration. However, there is still a large number of states. In this context, the mathematical

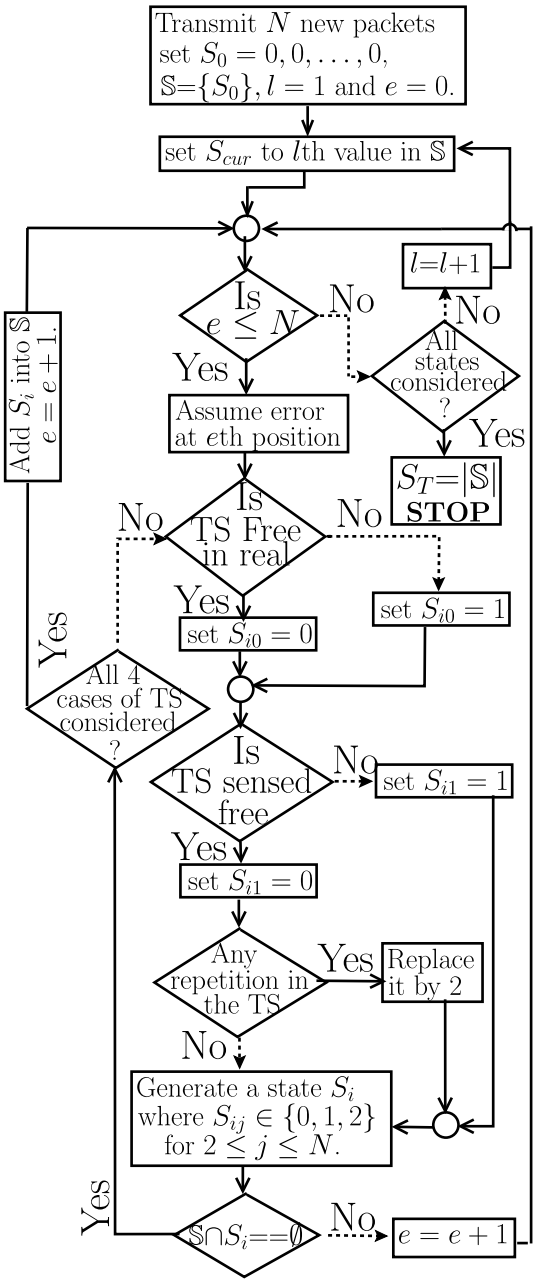

FIGURE 11. Illustration of the process of deriving states relaying on $(N + 2)$-length base-3 digits. For each value of e, the following four cases are considered: 1) correct detection of a free PR channel, 2) correct detection of a busy PR channel, 3) mis-detection, and 4) false-alarm . A special case of a completely error-free packet is represented by $e = 0$, while in a TS, e denotes the position of the corrupted packet.

formulation required for deriving total number of states and for generating state sequences with the aid of general expression remains an open challenge. However, the transition probability for any pair of state can be readily derived. Hence, we propose the algorithm shown in Fig. 11 for finding the number of states and the state sequences. The algorithm is conceived as follows.

Fundamentally, this algorithm uses a search technique for finding the legitimate states. Initially, the transmitter is set to the state $S_0 = 000000$. Let the legitimate states form the set $\mathbb{S}$, which initially contains only S_0. In the process for generating new states, we arrange for an erroneous transmission to occur at each possible position of the packets sent in the TS for the current state S_0. Let us simultaneously assume that the next TS is either free or busy, which is correctly sensed, mis-detected or sensed subject to a false-alarm.

For example, during the TS T_1 of Fig. 7, only new packets are transmitted, which are correctly received. Hence ACK flags are fed back. In the algorithm, this case is represented by $e = 0$. Continuing this example, when the next TS is busy, but it is sensed to be free, 4 new packets are transmitted in TS T_2. Consequently, the state is changed to $S_{243} = 100000$. Moreover, in the same case of $e = 0$, it is possible that TS T_2 may be sensed to be busy due to false detection of a free PR channel or owing the correct detection of a busy PR channel. If this is the case, the current state changes to $S_{81} = 010000$ for the false-alarm or to $S_{324} = 110000$ for the correct detection, respectively. When a new state is generated, for instance S_{324}, it is then checked against the state-set $\mathbb{S}$. If state S_{324} is already in $\mathbb{S}$, it is ignored. Otherwise, S_{324} is added to the set $\mathbb{S}$. Similarly, by considering the cases of $e = 1$ to $e = N$, the algorithm will generate all legitimate states that the transmitter may encounter upon emerging from state S_0. Once all the error-free transmission to erroneous transmission scenarios of each packet in a TS have been considered, the algorithm is then activated for the next state in $\mathbb{S}$, which is S_{243} in the example considered in Fig. 7. The algorithm repeats all the above steps for the sake of deriving new legitimate states. Moreover, due to the properties of irreducibility and the aperiodic nature of the DTMC, the state generating algorithm stops, once each state in $\mathbb{S}$ has been examined as current state and no new state is generated. Finally, at the end of the algorithm, the cardinality of the set $\mathbb{S}$ gives the total number of states S_T, i.e. we have $S_T = |\mathbb{S}|$.

C. STATE TRANSITION PROBABILITY MATRIX

Let the state transition probability matrix be expressed as $\mathbf{P}$ and the state at the ith TS be represented by $S(i)$. Then, for the example of Fig. 9, we have $S(1) = S_0$, $S(2) = S_{257}$, $S(3) = S_{120}$ $S(4) = S_{363}$ and $S(5) = S_{39}$. Given the state S_i in TS m, we have $S(m) = S_i$. Then the probability $P_{i,j}$ of transition to the next state is S_j, i.e. $S(m + 1) = S_j$ can be expressed [30], [104] as:

$$\begin{aligned} P_{i,j} &= P\left\{S(m+1) = S_j \mid S(m) = S_i, \ldots, S(1) = S_0\right\} \\ &= P\{S(m+1) = S_j | S(m) = S_i\}, \end{aligned} \tag{16}$$

which is the $(j, i)th$ element of $\mathbf{P}$. According to the properties of the DTMC, we have

$$\begin{aligned} 0 \leq P_{i,j} \leq 1 \\ \sum_{S_j \in \mathbb{S}} P_{i,j} = 1, \quad \forall\, S_i \in \mathbb{S}. \end{aligned} \tag{17}$$

It is worth noting that the transition probability $P_{i,j}$ is set to zero, if the transmitter cannot make a transition from S_i

to S_j in a single step (i.e. in the next TS). To continue our modelling, let the probability $P_i(m)$ represent the transmitter state in TS m. Then we have $\sum_{i\in\mathbb{S}} P_i(m) = 1$. Again, let $\boldsymbol{p}(m) = [P_0(m), P_1(m), \ldots, P_{S_T}(m)]^T$ store the S_T probabilities in TS m. Furthermore, we assume that the transmission commences from state $S(1) = S_0$ associated with the probabilities of

$$\boldsymbol{p}(1) = [1, 0, \ldots, 0]^T. \tag{18}$$

Then, with the aid of the law of total probability [30], [105], the specific probability that the Markov chain transitions into state j during the TS $(m+1)$ may readily be expressed as

$$P_j(m+1) = \sum_{\forall S_i\in\mathbb{S}} P_i(m)P_{i,j}, \quad \forall\, S_j \in \mathbb{S} \text{ and } m > 1. \tag{19}$$

By considering all the states in $\mathbb{S}$, we readily arrive at the recursive equation of

$$\boldsymbol{p}(m+1) = \mathbf{P}^T\boldsymbol{p}(m), \quad m = 1, 2, 3, 4, \ldots \tag{20}$$

given the above equation, we know that

$$\boldsymbol{p}(m+1) = (\mathbf{P}^T)^m\boldsymbol{p}(1). \tag{21}$$

Eq (17) shows that the state transition probability matrix $\mathbf{P}^T$ is a left stochastic matrix [105], because the sum of each column is equal to one. Consequently, based on the *Perron-Frobenius theorem*, the limit of $\lim_{m\to\infty}(\mathbf{P}^T)^m$ exists [105], and when we have $m \to \infty$, the DTMC reaches its steady state [30], implying that

$$\boldsymbol{p}(m+1) = \boldsymbol{p}(m). \tag{22}$$

Let us represent the steady-state probabilities by $\boldsymbol{\pi}$, i.e. $\boldsymbol{\pi} = \lim_{m\to\infty}\boldsymbol{p}(m)$. Then, based on (20) and (22), we have [30], [104],

$$\boldsymbol{\pi} = \mathbf{P}^T\boldsymbol{\pi}, \tag{23}$$

where $\boldsymbol{\pi}$ is the right eigenvector of $\mathbf{P}^T$, having an eigenvalue of one. As a result, the steady-state vector $\boldsymbol{\pi}$ can be found by determining the eigenvector of $\mathbf{P}^T$ [30], [104], [105].

D. THROUGHPUT OF CGBN-HARQ

The throughput of the CGBN-HARQ scheme is quantified in terms of the average number of packets successfully transmitted per TS. The successful transmission of a packet in a TS depends on two factors: 1) a free PR TS is correctly sensed by the CR system, and 2) the packet is delivered error-freely. As shown in (23), when the DTMC reaches its steady state, the throughput is determined by those states, which have one or more new packets successfully transmitted. Let us analyze the throughput in detail as follows.

As mentioned above, when the DTMC reaches its steady state, the additional throughput generated during the TS considered depends on two factors: 1) the PR channel is sensed free, corresponding to the scenario, when the first and second digits in the state sequence are either 00 or 10; and 2) the transmission of new packets in a respective state, provided that the channel is sensed to be free. Let us assume that $n_p(S_i)$ is the number of new packets transmitted in association with state $S_i \in \mathbb{S}_N$. Explicitly, $n_p(S_i)$ equals the number of zeros in the state sequence of S_i minus two, when the first two digits are 00 or minus one, if the first two digits are 10. Considering the first event, let us collect the states with the first two digits being 00 or 10 into a set denoted as $\mathbb{S}_N$. Then, when we obtained the steady state probabilities $\boldsymbol{\pi}$, the throughput of the CGBN-HARQ scheme can be evaluated as

$$R_T = \sum_{S_i\in\mathbb{S}_N} \pi_i \times n_p(S_i), \quad \text{(packets / TS)}. \tag{24}$$

Furthermore, if we express the throughput in terms of the number of packets per T_p (packet duration), we have

$$R'_T = \frac{T_p}{T} \times R_T = \frac{1}{k+N} \times R_T \quad \text{(packets / } T_p\text{)}. \tag{25}$$

Let us now analyze the delay imposed by our CGBN-HARQ scheme.

E. DELAY OF CGBN-HARQ

In the traditional GBN-HARQ, the transmission delay of a packet is contributed by the time required for its first transmission as well as the time associated with its retransmission. By contrast, in the proposed CGBN-HARQ, in addition to the above delay, extra delay may be imposed by the unavailability of the PR channel, which may either be due to the correct sensing of the busy PR channel or owing to the false sensing of the free PR channel. Therefore, in our CGBN-HARQ scheme [20], it is desirable to consider two types of delays, namely, the average packet delay and end-to-end packet delay. Specifically, the average packet delay may be defined as the total time required from the instant of sensing a TS until the error-free transmission of all packets divided by the total number of packets that had to be transmitted during this time. On the other hand, the end-to-end delay is the delay of a packet from its first transmission attempt until the instant that it is finally correctly received. Below we consider both types of delays.

1) AVERAGE PACKET DELAY

In the previous section, we have obtained the throughput quantified in terms of the average number of the packets per TS (or T_p). Hence, given the throughput as expressed in (24) or (25), we can readily infer that the average packet delay can be evaluated as

$$T_D = \frac{1}{R_s} \text{ (TS per packet)} \tag{26}$$

$$= \frac{k+N}{R_T} \text{ (T_p per packet)}. \tag{27}$$

2) END-TO-END PACKET DELAY

In this subsection, we will first commence by studying the probability mass function (PMF) of the end-to-end packet delay and then investigate the average end-to-end packet delay.

Let us define $\mathbb{S}_N$ for storing all the states in which one or more new packets are transmitted. In other words, $\mathbb{S}_N \subset \mathbb{S}$. Given a state $S_i \in \mathbb{S}_N$, we define another set $\mathbb{S}_i^{(m)}$ for accumulating the specific states $\{S_j\}$ in which $l_{i,j} \geq 1$ new packets transmitted from state S_i are correctly received with a delay of mT_p, i.e. we have:

$$\mathbb{S}_i^{(m)} = \{S_j |\ l_{i,j} \geq 1 \text{ new packets transmitted at state } S_i \text{ are correctly received at state state } S_j \text{ with exactly the delay of } mT_p\}. \quad (28)$$

Let L_i represents the number of new packets transmitted from S_i. Then, the PMF of the end-to-end packet delay can be evaluated as:

$$P(m) = \frac{1}{c} \sum_{S_i \in \mathbb{S}_N} \sum_{S_j \in \mathbb{S}_i^{(m)}} \frac{\pi_i \times l_{i,j} \times P_{i,j}^{(m)}}{L_i}, \quad m = 1, 2, \ldots. \quad (29)$$

where $c = \sum_{S_i \in \mathbb{S}_N} \pi_i$ and $P_{i,j}^{(m)}$ denotes the probability of transition from state S_i to state S_j with the delay of mT_p.

Given $\boldsymbol{\pi}$, $\boldsymbol{P}$ and $\mathbb{S}$, the PMF of end-to-end packet delay can be obtained as follows. Let

$$\boldsymbol{P}_{MF} = [P(1), P(2), \ldots, P(M_T)]^T, \quad (30)$$

where M_T represents the maximum delay having a very high value such as, 10^{-8}. Using this approximation, the probability of events having a delay higher than M_T can be ignored. Let us first initialize $\boldsymbol{p}^{(0)} = \boldsymbol{I}_i$, where $\boldsymbol{I}_i$ is the ith column of the identity matrix $\boldsymbol{I}_{S_T}$. Then, based on the properties of the DTMC, we have

$$\boldsymbol{p}^{(j)} = \mathbf{P}^T . \boldsymbol{p}^{(j-1)} = (\mathbf{P}^T)^j \boldsymbol{I}_i,\ j = 1, 2, \ldots \quad (31)$$

From (31) we can obtain the following insights:

a) If a packet originally transmitted in state S_i is successfully received in state S_j, the effective end-to-end delay is $jT_p s$;
b) The probabilities of transition from state S_i to any other states in $\mathbb{S}$ are given by $\boldsymbol{p}^{(j)}$ in (31);

Therefore, with the aid of the above information, we can update $\boldsymbol{P}_{MF}$ using the following formula:

$$P(m) \leftarrow P(m-1) + \frac{\pi_i \times l_{i,j} \times P_{i,j}^{(m)}}{L_i}, \quad (32)$$

for $m = 1, 2 \ldots, M_T$, $S_j \in \mathbb{S}_i^{(m)}$, $S_i \in \mathbb{S}_N$. Having formulated the PMF of the end-to-end packet delay, we now evaluate the average end-to-end packet delay as follows

$$\tau = \sum_{i=1}^{M_T} iT_p \times P(i). \quad (33)$$

Below we proceed by providing our performance results and validate our theoretical analysis by comparing the analytical results to those obtained from our simulations.

V. PERFORMANCE RESULTS

In this section, the performance of the CGBN-HARQ scheme is characterized, when both perfect and imperfect sensing are assumed. We quantify the throughput, the average packet delay and the average end-to-end packet delay. More specifically, we quantify the impact of false-alarm probability (P_{fa}), mis-detection probability (P_{md}), channel busy probability (P_{on}), packet error probability (P_e), as well as the number of packets N transmitted per TS. Note that in the perfect sensing environment of [20], both P_{fa} and P_{md} are zero.

For our simulations, we configure the CGBN-HARQ transmission scheme in Matlab in a realistic imperfect sensing environment, where the transmitter seamlessly transmits N packets in each free TS and the receiver generates feedback flags for the received packet. The PU's activity is based on a uniformly distributed random process. To analyse the performance of the CGBN-HARQ transmission scheme, we performed 50, 000 Monte Carlo simulations for all the parameters used in this study. Specifically, the parameters used in our simulations and in our theoretical modelling as well as their impact on the performance are summarized in Table 3. Furthermore, the observation period commences from the first TS and continues until the CR receiver successfully receives all packets. In our simulations, the period of observation commences from sensing the first TS and continues until the successful reception of all the packets considered. Correspondingly, the throughput is evaluated as

$$R_S' = \frac{N_s}{N_t \times (k+N)} \quad \text{(packets per } T_p\text{)}, \quad (34)$$

where N_t denotes the overall number of TSs required for the error-free transmission of N_s packets.

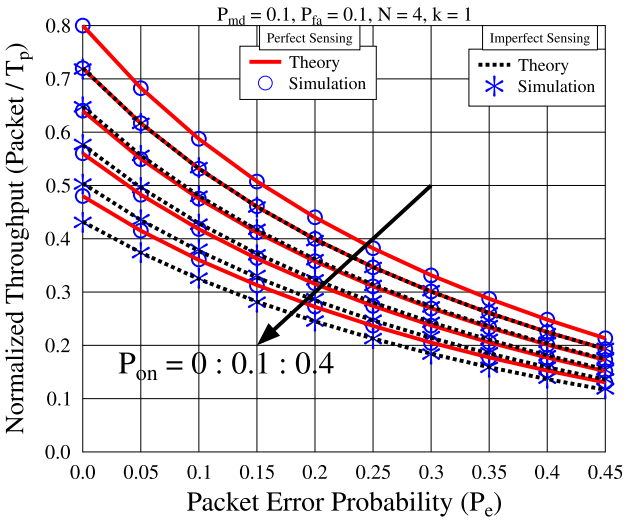

FIGURE 12. Throughput of the CGBN-HARQ versus P_e for various values of P_{on}, when $k = 1$ and $N = 4$. The theoretical results were calculated from (25) and the simulation results were obtained from (34).

Fig. 12 shows that for a given probability of P_{on}, the achievable throughput of CGBN-HARQ is at its maximum

TABLE 3. Performance parameters invoked in both the analytical and simulation-based modelling for the sake of quantifying the throughput (R_T), average packet delay (T_D), and average end-to-end packet delay (τ) of the CGBN-HARQ scheme in terms of packets transmission (N) per TS. The results shown are normalized to the unit of T_p and to the sensing duration of T_p while $P_{md} = 0.2$ and $P_{fa} = 0.2$. (a) For $P_{on} = 0$. (b) For $P_{on} = 0.2$. (c) For $P_{on} = 0.4$.

(a) For $P_{on} = 0$

P_e	N	R_T	T_D	τ
0	1	0.4	2.5	1
	2	0.53	1.87	1
	3	0.6	1.67	1
	4	0.64	1.56	1
	5	0.67	1.5	1
	6	0.69	1.45	1
	7	0.7	1.42	1
0.2	1	0.32	3.1	1.6
	2	0.38	2.6	2.35
	3	0.37	2.63	3.4
	4	0.35	2.7	5.1
	5	0.33	3	7.3
	6	0.31	3.2	10.13
	7	0.28	3.5	13.5
0.4	1	0.24	4.15	2.66
	2	0.25	3.91	4.8
	3	0.23	4.35	7.8
	4	0.2	5	12.2
	5	0.17	5.6	18.1
	6	0.15	6.4	25.5
	7	0.14	7.12	34.6

(b) For $P_{on} = 0.2$

P_e	N	R_T	T_D	τ
0	1	0.32	3.13	1.18
	2	0.43	2.34	1.3
	3	0.48	2.1	1.4
	4	0.51	1.95	1.5
	5	0.53	1.87	1.6
	6	0.55	1.82	1.64
	7	0.56	1.78	1.7
0.2	1	0.26	3.9	1.9
	2	0.31	3.25	2.3
	3	0.30	3.28	4.4
	4	0.28	3.46	6.5
	5	0.27	3.7	9.3
	6	0.25	4	12.8
	7	0.23	4.3	17
0.4	1	0.19	5.2	3.3
	2	0.2	4.9	6.1
	3	0.18	5.44	10.1
	4	0.16	6.2	15.8
	5	0.14	7.1	23.4
	6	0.125	8	33
	7	0.11	9	44.4

(c) For $P_{on} = 0.4$

P_{on}	N	R_T	T_D	τ
0	1	0.24	4.14	1.5
	2	0.26	3.12	2
	3	0.36	2.8	2.2
	4	0.38	2.6	2.5
	5	0.4	2.5	2.8
	6	0.41	2.4	3.1
	7	0.42	2.3	3.4
0.2	1	0.17	5.23	2.6
	2	0.18	4.34	4.2
	3	0.23	4.36	6.3
	4	0.22	4.6	9.3
	5	0.2	4.9	13.12
	6	0.19	5.25	17.8
	7	0.18	5.6	23.3
0.4	1	0.14	7	4.4
	2	0.13	6.5	8.4
	3	0.14	7.25	14.1
	4	0.12	8.3	22.13
	5	0.1	9.4	32.6
	6	0.09	10.6	45.7
	7	0.08	12	61.4

in both idealistic perfect and realistic imperfect sensing scenarios, when the channel used by the CU is perfectly reliable, yielding $P_e = 0$. However, when the channel becomes less reliable, i.e. when P_e increases, the throughput reduces with P_e due to the increase in the number of packet retransmissions. As shown in Fig 12, at a given P_e, the highest throughput is attained, when the PR channel is always free to use, corresponding to $P_{on} = 0$. By contrast, when P_{on} increases, the throughput of the CGBN-HARQ system decreases, since less time is available for the CU to transmits its data. Moreover, Fig 12 demonstrates the effect of unreliable sensing on the throughput, exhibiting a substantial drop due to the inaccurate sensing at a given P_e and/or P_{on}. Finally, as demonstrated in Fig 12, the results obtained from our analysis are validated by the simulation results, which confirms the accuracy of our analytical modelling.

Continuing with the throughput analysis now the optimal value of N is investigated in Fig. 13 versus P_e, P_{fa}, P_{md} and P_{on}. It can be seen that the throughput always increases upon increasing the value of N, provided that the channel is perfectly reliable, i.e. we have $P_e = 0$. When P_e increases, an increased value of N may result in a reduced throughput. This is because for a large value of N the number of retransmissions increases, once there is even a single packet in error. Furthermore, as seen in Fig. 13, for a given packet error probability $P_e \geq 0$, there exists an optimum value for N, which results in the highest throughput. The optimum value of N reduces, as the packet error probability P_e increases.

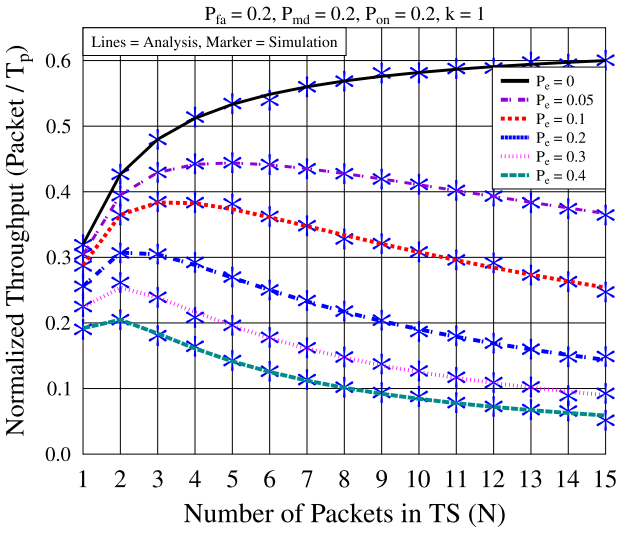

FIGURE 13. Investigating the optimal throughput of the CGBN-HARQ scheme based on the number of packet transmission (N) per TS, for various values of P_e in a perfect sensing environment.

Having characterized the attainable throughput, we now continue by quantifying the delay imposed. In our simulations, the average packet delay is computed as the total time duration required for the error-free transmission of N_s packets, divided by N_s, which is formulated as

$$T'_{DS} = \frac{N_t(k+N)}{N_s} \times T_p \text{ (seconds)}. \quad (35)$$

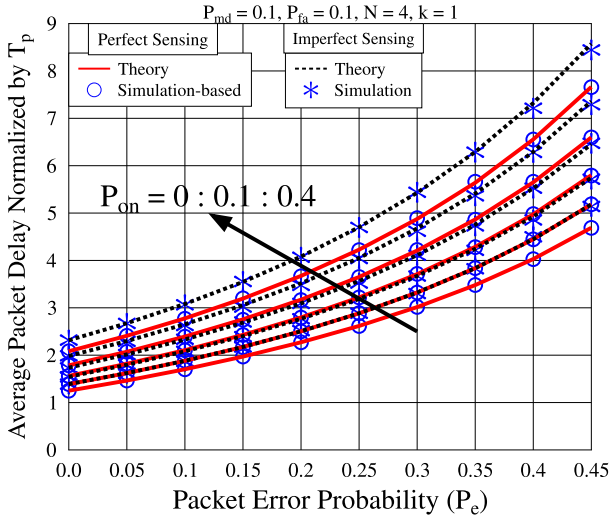

FIGURE 14. Average packet delay of the CGBN-HARQ system versus packet error probability for various channel busy probabilities when both perfect and imperfect sensing are considered. The theoretical results were calculated from (27), and the simulation results were obtained by taking into account the total number of TS used for transmission (35).

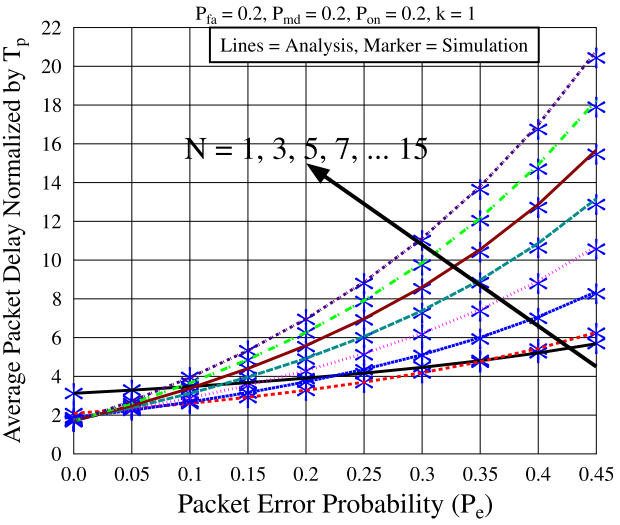

FIGURE 15. Investigating the optimal average packet delay of the CGBN-HARQ system based on the number of packets (N) per TS versus P_e in a realistic imperfect sensing environment, when $P_{on} = 0.2$ and $T_s = T_p$.

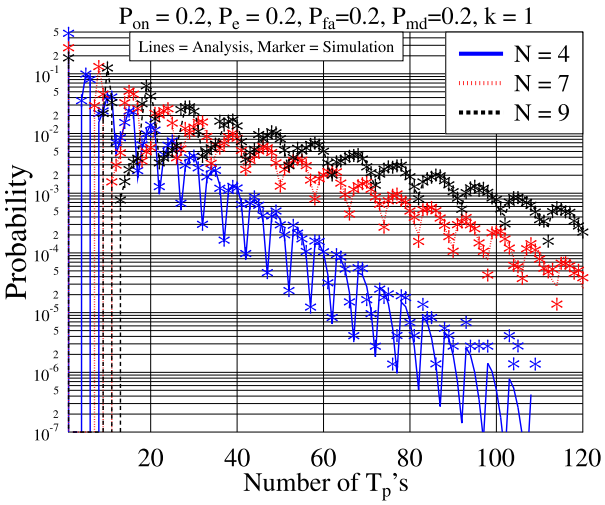

FIGURE 16. Probability distribution of end-to-end packet delay of the CGBN-HARQ systems in the case of imperfect sensing, when $P_{on} = 0.2$, $P_e = 0.2$, and $N = 4$, 7, and 9. The theoretical results were calculated from (32), and the simulation results were obtained by taking into account (36).

The results presented in Figs. 14 and 15 are normalized by T_p.

Specifically, Fig. 14 shows the average packet delay versus the packet error probability P_e, parametrized b the channel busy probability P_{on}. As shown in Fig. 14, the minimum delay is observed, when the channel is ideal, i.e. when $P_e = 0$ and/or when the channel is always free for the CU to use, corresponding to $P_{on} = 0$. The average packet delay increases upon increasing P_e and/or of P_{on}, as a result of the increased number of retransmissions and/or the reduced transmission opportunities for the CU. Furthermore, similar to the above discussions, the unreliable sensing also increases the average packet delay by deeming a free TS to be busy. By contrast, activating packet transmissions in a busy TS also increases the average packet delay due to the increase in the number of erroneous receptions and retransmissions. Additionally, as shown in Fig. 14 and also in Fig. 15, the results of our analytical approach are validated by the simulation results.

In Fig. 15, the average packet delay versus P_e relationship is characterized in terms of the number of packets transmitted in a single TS, given P_e, P_{fa}, P_{md} and P_{on}. As shown in the figure, at $P_e = 0$, a higher value of N gives a lower delay. However, when P_e is sufficiently large, a higher value of N results in a higher delay. For a given value of N, the average packet delay increases, as the channel becomes less reliable, i.e. when P_e increases. Again, as shown in Fig. 15, the simulation results validate our analytical results.

In Fig. 16, the PMF of the *end-to-end packet delay* is quantified for $N = 4, 7$ and 9, when realistic unreliable sensing is considered. In our simulation-based study the end-to-end delay of a packet is quantified in terms of the time duration spanning from its first transmission to the instant, when it is correctly received. Specifically, let the vector $\boldsymbol{d}$ of length N_s store the end-to-end delay in terms of T_p of the N_s packets, where N_s is a large number and $d(j)$ denotes the end-to-end delay of the jth packet. Hence, the PMF of the end-to-end packet delay presented in Fig. 16 is evaluated as

$$\boldsymbol{P}_d(i) = \frac{\sum_{j=1}^{N_s} \delta\left[d(j) - i\right]}{N_s}, \quad 1 \le i \le \max(\boldsymbol{d}), \qquad (36)$$

where $\max(\boldsymbol{d})$ denotes the maximum delay of the N_s packets. Note that in Fig. 16 the PMF associated with a delay beyond $120T_p's$ is not shown, since the values are all close to zero.

We observe from Fig. 16 that for the given parameter values and $N = 4$, 47.7% of the packets are successfully received after their first transmission. For the packets that are successfully received after their second transmissions, there are two cases. In the first case, if the TS following the

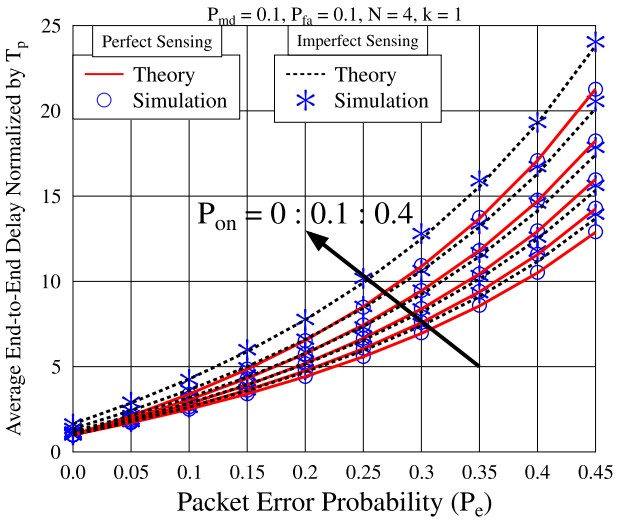

FIGURE 17. Average end-to-end packet delay versus P_e for various channel busy probabilities P_{on}, when both perfect and imperfect sensing are considered. The theoretical results were calculated from (33), and the simulation results were obtained by taking into account (37).

first transmission is free, on average 3.5%, 10% and 8.3% of the packets are successfully received with the delays of $4T_p$, $5T_p$ and $6T_p$, respectively. In the second case, if the TS during the first transmission is busy, then approximately 1.5%, 2.3%, 4.3% and 4.2% of the packets are successfully received with the delay of $8T_p$, $9T_p$, $10T_p$ and $11T_p$, respectively. Similarly, we can find the probabilities for the cases, when $N = 7$ and 9 are considered.

Having characterized the PMF of the end-to-end packet delay, we will now characterize the average-end-to-end packet delay of the CGBN-HARQ scheme. Here, the average end-to-end packet delay is formulated as:

$$\tau = \sum_{i=1}^{max(\boldsymbol{d})} \boldsymbol{P}_d(i) \times i(T_p). \tag{37}$$

Fig. 17 depicts the average end-to-end packet delay for $N = 4$ versus P_e and P_{on}, when both perfect and imperfect sensing are considered. Similar to the trends observed in the analysis of the average packet delay, the average end-to-end packet delay increases with P_e and/or P_{on}. However, when comparing Fig. 14 and 17, there are two main noticeable characteristics associated with the minimum delays and with the delay-gradient. Firstly, in terms of the minimum delays, observe in Fig. 17 at $P_e = 0$ that the minimum end-to-end packet delay is one T_p in the case of perfect sensing, regardless of the channel's busy probability of P_{on}. In the case of imperfect sensing, the minimum delay increases to an average of 1.6 T_p, when $P_{on} = 0.4$. By contrast, we observed from Fig. 14 that the average packet delay has a higher than a one T_p interval minimum delay, which further increases upon increasing in P_{on}, regardless of using perfect or imperfect sensing. The reason for this observation is that the average packet delay includes the busy time before a packet's transmission. By contrast, the end-to-end packet delay is calculated for each of packet individually, spanning from the instant of its first transmission attempt until its successful reception. Secondly, upon comparing Fig. 17 to Fig. 14, we observe that the average end-to-end packet delay gradient is higher than that of the average packet delay as a function of P_e and/or P_{on}. This is because in the CGBN-HARQ scheme the delay of every transmitted packet is dependent on the success of $(N-1)$ packets transmitted a head of it. Therefore, if any of the $(N-1)$ previous packet is corrupted, then all the respective packets have to be retransmitted, regardless whether they are error-free. This phenomenon results in longer end-to-end packet delays.

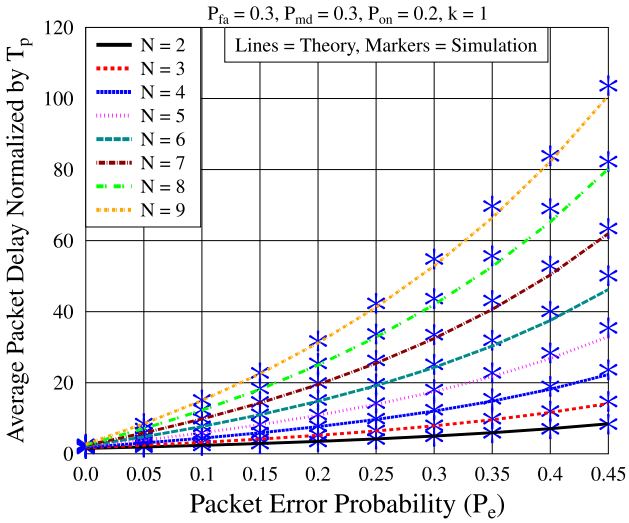

FIGURE 18. The optimal average end-to-end packet delay of the CGBN-HARQ system based on the number of packets (N) versus P_e in the scenario of imperfect sensing.

Moreover, in Fig. 18 we depict the effect of increasing the number packets per TS on the average end-to-end packet delay. Explicitly, for a given value of P_e, the average end-to-end packet delay increases, as the value of N increases. Furthermore, at a given P_e, the gradient of the average end-to-end delay curve increases, as the value of N becomes higher.

VI. CONCLUSIONS

In this paper, we investigated a CGBN-HARQ transmission scheme conceived for CR systems, when both reliable and unreliable sensing are considered. Both the throughput and delay of CGBN-HARQ has been investigated both by analysis and simulations. The CGBN-HARQ system was modelled using DTMC-based approach, based on which closed-form expressions have been derived both for the throughput and for the delay. Both the average packet delay and the average end-to-end packet delay have been studied. Finally, our analytical results have been validated by our simulation results. The performance results of the CGBN-HARQ recorded for idealistic and realistic sensing environments were compared. The results presented in the above figures are summarized in Table 3, which reveals that the reliability of spectrum

sensing, the activity of the PUs and the reliability of the CR communication have a substantial impact on the throughput and delay of the CGBN-HARQ transmission scheme. When the CR communication become less reliable or when the PU has a high probability of exploiting the channel, the throughput reduces significantly, which ultimately results in an increased transmission delay. Additionally, the optimal value of the throughput and delay of CGBN-HARQ have been quantified in terms of the number of packets transmitted per TS. This quantitative analysis reveals that when the propagation environment is time-variant, the number of packets transmitted within a TS should be appropriately adapted for achieving the highest possible throughput and the shortest average transmission delay.

REFERENCES

[1] J. Mitola and G. Q. Maguire, Jr., "Cognitive radio: Making software radios more personal," *IEEE Pers. Commun.*, vol. 6, no. 4, pp. 13–18, Apr. 1999.

[2] "Spectrum policy task force," Federal Commun. Commission, Washington, Dc, USA, Tech. Rep. Et Docket 02-155, Nov. 2002.

[3] G. Staple and K. Werbach, "The end of spectrum scarcity [spectrum allocation and utilization]," *IEEE Spectr.*, vol. 41, no. 3, pp. 48–52, Mar. 2004.

[4] J. Yang, "Spatial channel characterization for cognitive radios," M.S. thesis, Dept. Elect. Eng. Comput. Sci., Univ. California, Berkeley, Berkeley, CA, USA, Jan. 2005. [Online]. Available: http://www.eecs.berkeley.edu/Pubs/TechRpts/2005/4293.html

[5] M. A. McHenry, P. A. Tenhula, D. McCloskey, D. A. Roberson, and C. S. Hood, "Chicago spectrum occupancy measurements & analysis and a long-term studies proposal," in *Proc. 1st Int. Workshop Technol. Policy Accessing Spectr. (TAPAS)*, 2006, Art. no. 1.

[6] Q. Zhao and B. M. Sadler, "A survey of dynamic spectrum access," *IEEE Signal Process. Mag.*, vol. 24, no. 3, pp. 79–89, May 2007.

[7] E. Hossain, D. Niyato, and Z. Han, *Dynamic Spectrum Access and Management in Cognitive Radio Networks*. Cambridge, U.K.: Cambridge Univ. Press, 2009.

[8] S. Haykin, "Cognitive radio: Brain-empowered wireless communications," *IEEE J. Sel. Areas Commun.*, vol. 23, no. 2, pp. 201–220, Feb. 2005.

[9] I. F. Akyildiz, W.-Y. Lee, M. C. Vuran, and S. Mohanty, "Next generation/dynamic spectrum access/cognitive radio wireless networks: A survey," *Comput. Netw.*, vol. 50, no. 13, pp. 2127–2159, Sep. 2006.

[10] "Second report and order," Federal Commun. Commission, Washington, Dc, USA, Tech. Rep. Et Docket 08-260, Nov. 2008.

[11] "Notice of proposed rule making, in the matter of unlicensed operation in the TV broadcast bands and order (ET Docket No 04-186) and additional spectrum for unlicensed devices below 900 MHz and in the 3 GHz band," Federal Commun. Commission, Tech. Rep. ET Docket 02-380, May 2004.

[12] M. Sherman, A. N. Mody, R. Martinez, C. Rodriguez, and R. Reddy, "IEEE standards supporting cognitive radio and networks, dynamic spectrum access, and coexistence," *IEEE Commun. Mag.*, vol. 46, no. 7, pp. 72–79, Jul. 2008.

[13] I. F. Akyildiz, W.-Y. Lee, M. C. Vuran, and S. Mohanty, "A survey on spectrum management in cognitive radio networks," *IEEE Commun. Mag.*, vol. 46, no. 4, pp. 40–48, Apr. 2008.

[14] E. Z. Tragos, S. Zeadally, A. G. Fragkiadakis, and V. A. Siris, "Spectrum assignment in cognitive radio networks: A comprehensive survey," *IEEE Commun. Surveys Tut.*, vol. 15, no. 3, pp. 1108–1135, 3rd Quart., 2013.

[15] S. Lin and D. J. Costello, Jr., *Error Control Coding: Fundamentals and Applications*, 2nd ed. Upper Saddle River, NJ, USA: Prentice-Hall, 1999.

[16] L. Hanzo, T. H. Liew, B. L. Yeap, R. Y. S. Tee, and S. X. Ng, *Turbo Coding, Turbo Equalisation and Space-Time Coding: Exit-Chart-Aided Near-Capacity Designs for Wireless Channels*, 2nd ed. Hoboken, NJ, USA: Wiley, 2011.

[17] A. U. Rehman, L.-L. Yang, and L. Hanzo, "Performance of cognitive hybrid automatic repeat request: Stop-and-wait," in *Proc. IEEE 81st Veh. Technol. Conf. (VTC Spring)*, May 2015, pp. 1–5.

[18] A. U. Rehman, C. Dong, L.-L. Yang, and L. Hanzo, "Performance of cognitive stop-and-wait hybrid automatic repeat request in the face of imperfect sensing," *IEEE Access*, vol. 4, pp. 5489–5508, Jul. 2016.

[19] A. U. Rehman, L.-L. Yang, and L. Hanzo, "Performance of cognitive hybrid automatic repeat request: Go-Back-N," in *Proc. IEEE 83rd Veh. Technol. Conf. (VTC Spring)*, May 2016, pp. 1–5.

[20] A. U. Rehman, C. Dong, V. A. Thomas, L.-L. Yang, and L. Hanzo, "Throughput and delay analysis of cognitive Go-Back-N hybrid automatic repeat request using discrete-time Markov modelling," *IEEE Access*, to be published.

[21] A. U. Rehman, V. A. Thomas, L.-L. Yang, and L. Hanzo, "Performance of cognitive selective-repeat hybrid automatic repeat request," *IEEE Access*, to be published.

[22] G. Ozcan and M. C. Gursoy, "Throughput of cognitive radio systems with finite blocklength codes," *IEEE J. Sel. Areas Commun.*, vol. 31, no. 11, pp. 2541–2554, Nov. 2013.

[23] H. Su and X. Zhang, "Cross-layer based opportunistic MAC protocols for QoS provisionings over cognitive radio wireless networks," *IEEE J. Sel. Areas Commun.*, vol. 26, no. 1, pp. 118–129, Jan. 2008.

[24] W. Y. Lee and I. F. Akyildiz, "Optimal spectrum sensing framework for cognitive radio networks," *IEEE Trans. Wireless Commun.*, vol. 7, no. 10, pp. 3845–3857, Oct. 2008.

[25] S. Akin and M. C. Gursoy, "Performance analysis of cognitive radio systems under QoS constraints and channel uncertainty," *IEEE Trans. Wireless Commun.*, vol. 10, no. 9, pp. 2883–2895, Sep. 2011.

[26] Y. Saleem and M. H. Rehmani, "Primary radio user activity models for cognitive radio networks: A survey," *J. Netw. Comput. Appl.*, vol. 43, pp. 1–16, Aug. 2014.

[27] Y.-C. Liang, Y. Zeng, E. C. Y. Peh, and A. T. Hoang, "Sensing-throughput tradeoff for cognitive radio networks," *IEEE Trans. Wireless Commun.*, vol. 7, no. 4, pp. 1326–1337, Apr. 2008.

[28] X. Kang, Y. C. Liang, H. K. Garg, and L. Zhang, "Sensing-based spectrum sharing in cognitive radio networks," *IEEE Trans. Veh. Technol.*, vol. 58, no. 8, pp. 4649–4654, Oct. 2009.

[29] S. Stotas and A. Nallanathan, "Enhancing the capacity of spectrum sharing cognitive radio networks," *IEEE Trans. Veh. Technol.*, vol. 60, no. 8, pp. 3768–3779, Oct. 2011.

[30] D. Bertsekas and R. Gallagher, *Data Networks*, 2nd ed. Englewood Cliffs, NJ, USA: Prentice-Hall, 1991.

[31] R. Fantacci, "Queuing analysis of the selective repeat automatic repeat request protocol wireless packet networks," *IEEE Trans. Veh. Technol.*, vol. 45, no. 2, pp. 258–264, May 1996.

[32] L. Badia, M. Rossi, and M. Zorzi, "SR ARQ packet delay statistics on Markov channels in the presence of variable arrival rate," *IEEE Trans. Wireless Commun.*, vol. 5, no. 7, pp. 1639–1644, Jul. 2006.

[33] A. R. K. Sastry, "Improving automatic repeat-request (ARQ) performance on satellite channels under high error rate conditions," *IEEE Trans. Commun.*, vol. 23, no. 4, pp. 436–439, Apr. 1975.

[34] S. Lin, D. J. Costello, and M. J. Miller, "Automatic-repeat-request error-control schemes," *IEEE Commun. Mag.*, vol. 22, no. 12, pp. 5–17, Dec. 1984.

[35] J. Du, M. Kasahara, and T. Namekawa, "Separate codes on type-II hybrid ARQ systems," *IEEE Trans. Commun.*, vol. 36, no. 10, pp. 1089–1097, Oct. 1988.

[36] S. Kallel, "Analysis of a type II hybrid ARQ scheme with code combining," *IEEE Trans. Commun.*, vol. 38, no. 8, pp. 1133–1137, Aug. 1990.

[37] P. Decker, "An adaptive type-II hybrid ARQ/FEC protocol suitable for GSM," in *Proc. IEEE 44th Veh. Technol. Conf.*, vol. 1. Jun. 1994, pp. 330–333.

[38] M. Zorzi, R. R. Rao, and L. B. Milstein, "ARQ error control for fading mobile radio channels," *IEEE Trans. Veh. Technol.*, vol. 46, no. 2, pp. 445–455, May 1997.

[39] J. Hamorsky and L. Hanzo, "Performance of the turbo hybrid automatic repeat request system type II," in *Proc. Inf. Theory Netw. Workshop*, Jun./Jul. 1999, p. 51.

[40] E. M. Sozer, M. Stojanovic, and J. G. Proakis, "Underwater acoustic networks," *IEEE J. Ocean. Eng.*, vol. 25, no. 1, pp. 72–83, Jan. 2000.

[41] G. Caire and D. Tuninetti, "The throughput of hybrid-ARQ protocols for the Gaussian collision channel," *IEEE Trans. Inf. Theory*, vol. 47, no. 5, pp. 1971–1988, Jul. 2001.

[42] W. T. Kim, S. J. Bae, J. G. Kim, and E. K. Joo, "Performance of STBC with turbo code in HARQ scheme for mobile communication systems," in *Proc. 10th Int. Conf. Telecommun. (ICT)*, vol. 1. Feb. 2003, pp. 85–89.
[43] B. Zhao and M. C. Valenti, "Practical relay networks: A generalization of hybrid-ARQ," *IEEE J. Sel. Areas Commun.*, vol. 23, no. 1, pp. 7–18, Jan. 2005.
[44] K. C. Beh, A. Doufexi, and S. Armour, "Performance evaluation of hybrid ARQ schemes of 3GPP LTE OFDMA system," in *Proc. IEEE 18th Int. Symp. Pers., Indoor Mobile Radio Commun.*, Sep. 2007, pp. 1–5.
[45] M. C. Vuran and I. F. Akyildiz, "Error control in wireless sensor networks: A cross layer analysis," *IEEE/ACM Trans. Netw.*, vol. 17, no. 4, pp. 1186–1199, Aug. 2009.
[46] R. Zhang and L. Hanzo, "Superposition-aided delay-constrained hybrid automatic repeat request," *IEEE Trans. Veh. Technol.*, vol. 59, no. 4, pp. 2109–2115, May 2010.
[47] R. Zhang and L. Hanzo, "A unified treatment of superposition coding aided communications: Theory and practice," *IEEE Commun. Surveys Tut.*, vol. 13, no. 3, pp. 503–520, 3rd Quart., 2011.
[48] H. Chen, R. G. Maunder, and L. Hanzo, "Low-complexity multiple-component turbo-decoding-aided hybrid ARQ," *IEEE Trans. Veh. Technol.*, vol. 60, no. 4, pp. 1571–1577, May 2011.
[49] H. Chen, R. G. Maunder, and L. Hanzo, "Lookup-table-based deferred-iteration aided low-complexity turbo hybrid ARQ," *IEEE Trans. Veh. Technol.*, vol. 60, no. 7, pp. 3045–3053, Sep. 2011.
[50] H. Chen, R. G. Maunder, and L. Hanzo, "Deferred-iteration aided low-complexity turbo hybrid ARQ relying on a look-up table," in *Proc. IEEE Global Telecommun. Conf. (GLOBECOM)*, Dec. 2011, pp. 1–5.
[51] H. Chen, R. G. Maunder, and L. Hanzo, "A survey and tutorial on low-complexity turbo coding techniques and a holistic hybrid ARQ design example," *IEEE Commun. Surveys Tut.*, vol. 15, no. 4, pp. 1546–1566, 4th Quart., 2013.
[52] B. Zhang, H. Chen, M. El-Hajjar, R. Maunder, and L. Hanzo, "Distributed multiple-component turbo codes for cooperative hybrid ARQ," *IEEE Signal Process. Lett.*, vol. 20, no. 6, pp. 599–602, Jun. 2013.
[53] H. A. Ngo and L. Hanzo, "Hybrid automatic-repeat-request systems for cooperative wireless communications," *IEEE Commun. Surveys Tut.*, vol. 16, no. 1, pp. 25–45, 1st Quart., 2014.
[54] M. Chitre and W.-S. Soh, "Reliable point-to-point underwater acoustic data transfer: To juggle or not to juggle?" *IEEE J. Ocean. Eng.*, vol. 40, no. 1, pp. 93–103, Jan. 2015.
[55] K. Xu *et al.*, "NTC-HARQ: Network–turbo-coding based HARQ protocol for wireless broadcasting system," *IEEE Trans. Veh. Technol.*, vol. 64, no. 10, pp. 4633–4644, Oct. 2015.
[56] C. Zhu, Y. Huo, B. Zhang, R. Zhang, M. El-Hajjar, and L. Hanzo, "Adaptive-truncated-HARQ-aided layered video streaming relying on interlayer FEC coding," *IEEE Trans. Veh. Technol.*, vol. 65, no. 3, pp. 1506–1521, Mar. 2016.
[57] B. Makki, T. Eriksson, and T. Svensson, "On the performance of the relay–ARQ networks," *IEEE Trans. Veh. Technol.*, vol. 65, no. 4, pp. 2078–2096, Apr. 2016.
[58] A. Leon-Garcia and I. Widjaja, *Communication Networks*. New York, NY, USA: McGraw-Hill, 2004.
[59] Y. Hayashida and M. Komatsu, "Delay performance of Go-Back-N ARQ scheme with Markovian error channel," in *Proc. 2nd Int. Conf. Pers. Commun., Gateway 21st Century*, vol. 1. Oct. 1993, pp. 448–452.
[60] M. Zorzi and R. R. Rao, "Performance of ARQ Go-Back-N protocol in Markov channels with unreliable feedback: Delay analysis," in *Proc. IEEE 4th Int. Conf. Universal Pers. Commun.*, Nov. 1995, pp. 481–485.
[61] W. Turin, "Throughput analysis of the Go-Back-N protocol in fading radio channels," *IEEE J. Sel. Areas Commun.*, vol. 17, no. 5, pp. 881–887, May 1999.
[62] S. S. Chakraborty and M. Liinaharja, "On the performance of an adaptive GBN scheme in a time-varying channel," *IEEE Commun. Lett.*, vol. 4, no. 4, pp. 143–145, Apr. 2000.
[63] M. Zorzi, "Some results on error control for burst-error channels under delay constraints," *IEEE Trans. Veh. Technol.*, vol. 50, no. 1, pp. 12–24, Jan. 2001.
[64] K. Ausavapattanakun and A. Nosratinia, "Analysis of Go-Back-N ARQ in block fading channels," *IEEE Trans. Wireless Commun.*, vol. 6, no. 8, pp. 2793–2797, Aug. 2007.
[65] C. Dong, L.-L. Yang, J. Zuo, S. X. Ng, and L. Hanzo, "Energy, delay, and outage analysis of a buffer-aided three-node network relying on opportunistic routing," *IEEE Trans. Commun.*, vol. 63, no. 3, pp. 667–682, Mar. 2015.
[66] C. Dong, L.-L. Yang, and L. Hanzo, "Performance of buffer-aided adaptive modulation in multihop communications," *IEEE Trans. Commun.*, vol. 63, no. 10, pp. 3537–3552, Oct. 2015.
[67] Y. Qin and L.-L. Yang, "Delay comparison of automatic repeat request assisted butterfly networks," in *Proc. 7th Int. Symp. Wireless Commun. Syst.*, Sep. 2010, pp. 686–690.
[68] Y. Qin and L.-L. Yang, "Throughput comparison of automatic repeat request assisted butterfly networks," in *Proc. 7th Int. Symp. Wireless Commun. Syst.*, Sep. 2010, pp. 581–585.
[69] Y. Qin and L.-L. Yang, "Throughput analysis of stop-and-wait automatic repeat request scheme for network coding nodes," in *Proc. IEEE 71st Veh. Technol. Conf. (VTC-Spring)*, May 2010, pp. 1–5.
[70] Y. Qin and L.-L. Yang, "Steady-state throughput analysis of network coding nodes employing stop-and-wait automatic repeat request," *IEEE/ACM Trans. Netw.*, vol. 20, no. 5, pp. 1402–1411, Oct. 2012.
[71] S. Li, Y. Zhou, X. Yang, and Z. Dou, "Performance evaluation of multiple relays cooperative gbn-arq with limited retransmission," *J. Syst. Eng. Electron.*, vol. 26, no. 6, pp. 1210–1215, Dec. 2015.
[72] R. E. Ramos and K. Madani, "A novel generic distributed intelligent re-configurable mobile network architecture," in *Proc. 53rd IEEE Veh. Technol. Conf. (VTC)*, vol. 3. May 2001, pp. 1927–1931.
[73] D. Cabric and R. W. Brodersen, "Physical layer design issues unique to cognitive radio systems," in *Proc. IEEE 16th Int. Symp. Pers., Indoor Mobile Radio Commun. (PIMRC)*, vol. 2. Sep. 2005, pp. 759–763.
[74] T. Fujii, Y. Kamiya, and Y. Suzuki, "Multi-band ad-hoc cognitive radio for reducing inter system interference," in *Proc. IEEE 17th Int. Symp. Pers., Indoor Mobile Radio Commun.*, Sep. 2006, pp. 1–5.
[75] N. Devroye, P. Mitran, and V. Tarokh, "Limits on communications in a cognitive radio channel," *IEEE Commun. Mag.*, vol. 44, no. 6, pp. 44–49, Jun. 2006.
[76] T. Weingart, D. C. Sicker, and D. Grunwald, "A statistical method for reconfiguration of cognitive radios," *IEEE Wireless Commun.*, vol. 14, no. 4, pp. 34–40, Aug. 2007.
[77] S.-L. Cheng and Z. Yang, "Cross-layer combining of power control and adaptive modulation with truncated ARQ for cognitive radios," *J. China Univ. Posts Telecommun.*, vol. 15, no. 3, pp. 19–23, 2008.
[78] G. Yue and X. Wang, "Anti-jamming coding techniques with application to cognitive radio," *IEEE Trans. Wireless Commun.*, vol. 8, no. 12, pp. 5996–6007, Dec. 2009.
[79] W.-C. Ao and K.-C. Chen, "End-to-end HARQ in cognitive radio networks," in *Proc. IEEE Wireless Commun. Netw. Conf. (WCNC)*, Apr. 2010, pp. 1–6.
[80] Y. Liu, Z. Feng, and P. Zhang, "A novel ARQ scheme based on network coding theory in cognitive radio networks," in *Proc. IEEE Int. Conf. Wireless Inf. Technol. Syst. (ICWITS)*, Aug. 2010, pp. 1–4.
[81] S.-M. Cheng, W. C. Ao, and K.-C. Chen, "Efficiency of a cognitive radio link with opportunistic interference mitigation," *IEEE Trans. Wireless Commun.*, vol. 10, no. 6, pp. 1715–1720, Jun. 2011.
[82] B. Makki, A. G. I. Amat, and T. Eriksson, "HARQ feedback in spectrum sharing networks," *IEEE Commun. Lett.*, vol. 16, no. 9, pp. 1337–1340, Sep. 2012.
[83] R. Andreotti, I. Stupia, V. Lottici, F. Giannetti, and L. Vandendorpe, "Goodput-based link resource adaptation for reliable packet transmissions in BIC-OFDM cognitive radio networks," *IEEE Trans. Signal Process.*, vol. 61, no. 9, pp. 2267–2281, May 2013.
[84] G. Ozcan, M. C. Gursoy, and S. Gezici, "Error rate analysis of cognitive radio transmissions with imperfect channel sensing," *IEEE Trans. Wireless Commun.*, vol. 13, no. 3, pp. 1642–1655, Mar. 2014.
[85] Y.-C. Chen, I.-W. Lai, K.-C. Chen, W.-T. Chen, and C.-H. Lee, "Transmission latency and reliability trade-off in path-time coded cognitive radio ad hoc networks," in *Proc. IEEE Global Commun. Conf.*, Dec. 2014, pp. 1084–1089.
[86] Y. Zou, J. Zhu, L. Yang, Y.-C. Liang, and Y.-D. Yao, "Securing physical-layer communications for cognitive radio networks," *IEEE Commun. Mag.*, vol. 53, no. 9, pp. 48–54, Sep. 2015.
[87] B. Makki, T. Svensson, and M. Zorzi, "Finite block-length analysis of spectrum sharing networks: Interference-constrained scenario," *IEEE Wireless Commun. Lett.*, vol. 4, no. 4, pp. 433–436, Aug. 2015.

[88] B. Makki, T. Svensson, and M. Zorzi, "Finite block-length analysis of spectrum sharing networks using rate adaptation," *IEEE Trans. Commun.*, vol. 63, no. 8, pp. 2823–2835, Aug. 2015.
[89] A. A. Khan, M. H. Rehmani, and M. Reisslein, "Cognitive radio for smart grids: Survey of architectures, spectrum sensing mechanisms, and networking protocols," *IEEE Commun. Surveys Tut.*, vol. 18, no. 1, pp. 860–898, 1st Quart., 2016.
[90] L. Zhang, M. Xiao, G. Wu, S. Li, and Y.-C. Liang, "Energy-efficient cognitive transmission with imperfect spectrum sensing," *IEEE J. Sel. Areas Commun.*, vol. 34, no. 5, pp. 1320–1335, May 2016.
[91] A. Patel, M. Z. A. Khan, S. N. Merchant, U. B. Desai, and L. Hanzo, "Achievable rates of underlay-based cognitive radio operating under rate limitation," *IEEE Trans. Veh. Technol.*, vol. 65, no. 9, pp. 7149–7159, Sep. 2016.
[92] A. Patel, Z. Khan, S. Merchant, U. Desai, and L. Hanzo, "The achievable rate of interweave cognitive radio in the face of sensing errors," *IEEE Access*, to be published.
[93] J. C. F. Li, W. Zhang, A. Nosratinia, and J. Yuan, "SHARP: Spectrum harvesting with ARQ retransmission and probing in cognitive radio," *IEEE Trans. Commun.*, vol. 61, no. 3, pp. 951–960, Mar. 2013.
[94] D. Hamza and S. Aissa, "Enhanced primary and secondary performance through cognitive relaying and leveraging primary feedback," *IEEE Trans. Veh. Technol.*, vol. 63, no. 5, pp. 2236–2247, Jun. 2014.
[95] J. S. Harsini and M. Zorzi, "Transmission strategy design in cognitive radio systems with primary ARQ control and QoS provisioning," *IEEE Trans. Commun.*, vol. 62, no. 6, pp. 1790–1802, Jun. 2014.
[96] S. Touati, H. Boujemaa, and N. Abed, "Cooperative ARQ protocols for underlay cognitive radio networks," in *Proc. 21st Eur. Signal Process. Conf. (EUSIPCO)*, Sep. 2013, pp. 1–5.
[97] G. Yue, X. Wang, and M. Madihian, "Design of anti-jamming coding for cognitive radio," in *Proc. IEEE Global Telecommun. Conf.*, Nov. 2007, pp. 4190–4194.
[98] G. Yue and X. Wang, "Design of efficient ARQ schemes with anti-jamming coding for cognitive radios," in *Proc. IEEE Wireless Commun. Netw. Conf. (WCNC)*, Apr. 2009, pp. 1–6.
[99] W. Liang, S. X. Ng, J. Feng, and L. Hanzo, "Pragmatic distributed algorithm for spectral access in cooperative cognitive radio networks," *IEEE Trans. Commun.*, vol. 62, no. 4, pp. 1188–1200, Apr. 2014.
[100] J. Hu, L. L. Yang, and L. Hanzo, "Maximum average service rate and optimal queue scheduling of delay-constrained hybrid cognitive radio in Nakagami fading channels," *IEEE Trans. Veh. Technol.*, vol. 62, no. 5, pp. 2220–2229, Jun. 2013.
[101] Y.-C. Liang, K.-C. Chen, G. Y. Li, and P. Mahonen, "Cognitive radio networking and communications: An overview," *IEEE Trans. Veh. Technol.*, vol. 60, no. 7, pp. 3386–3407, Sep. 2011.
[102] C. Cormio and K. R. Chowdhury, "A survey on MAC protocols for cognitive radio networks," *Ad Hoc Netw.*, vol. 7, no. 7, pp. 1315–1329, Sep. 2009.
[103] A. De Domenico, E. C. Strinati, and M.-G. Di Benedetto, "A survey on MAC strategies for cognitive radio networks," *IEEE Commun. Surveys Tut.*, vol. 14, no. 1, pp. 21–44, 1st Quart., 2012.
[104] R. A. Howard, *Dynamic Probabilistic Systems: Markov Models*. New York, NY, USA: Wiley, 1971.
[105] R. A. Horn and C. R. Johnson, *Matrix Analysis*. Cambridge, U.K.: Cambridge Univ. Press, 2012.

ATEEQ UR REHMAN received the B.Eng. degree in computer science and information technology from Islamic University of Technology, Dhaka, Bangladesh, in 2009, and the Ph.D. degree in wireless communications from the University of Southampton, Southampton, U.K., in 2016.

He is currently a Lecturer with the Department of Computer Science, Abdul Wali Khan University, Mardan, Pakistan. His main research interests are next-generation wireless communications and cognitive radio networks, co-operative communication, and resource allocation, particularly cross-layer approach and hybrid ARQ.

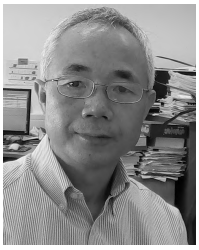

LIE-LIANG YANG (F'15) received the B.Eng. degree in communications engineering from Shanghai TieDao University, Shanghai, China, in 1988, and the M.Eng. and Ph.D. degrees in communications and electronics from Northern (Beijing) Jiaotong University, Beijing, China, in 1991 and 1997, respectively.

In 1997, he was a Visiting Scientist with the Institute of Radio Engineering and Electronics, Academy of Sciences of the Czech Republic. Since 1997, he has been with the University of Southampton, U.K., where he is currently a Professor of Wireless Communications with the School of Electronics and Computer Science. He has authored more than 330 research papers in journals and conference proceedings, authored or co-authored three books, and also published several book chapters. His research interest is in a wide range of topics in wireless communications, wireless networks and signal processing for wireless communications, and molecular communications. He is a fellow of the IET. He is a Distinguished Lecturer of the IEEE.

He served as an Associate Editor of the IEEE TRANSACTIONS ON VEHICULAR TECHNOLOGY and the *Journal of Communications and Networks*. He is currently an Associate Editor of the IEEE ACCESS and the *Security and Communication Networks* Journal.

LAJOS HANZO (F'08) received the D.Sc. degree in electronics in 1976 and the Ph.D. degree in 1983.

During his 35-year career in telecommunications, he has held various research and academic posts in Hungary, Germany, and the U.K. Since 1986, he has been with the School of Electronics and Computer Science, University of Southampton, U.K. He has successfully supervised in excess of 100 Ph.D. students. He is currently directing a 60-strong academic research team, working on a range of research projects in the field of wireless multimedia communications sponsored by industry, the Engineering and Physical Sciences Research Council, U.K., the European IST Programme, and the Mobile Virtual Centre of Excellence, U.K. His research is funded by the European Research Council's Senior Research Fellow Grant. He is an enthusiastic supporter of industrial and academic liaison, and he offers a range of industrial courses. He has co-authored 20 John Wiley/IEEE Press books on mobile radio communications totalling in excess of 10 000 pages, published over 1600 research entries on the IEEE Xplore.

Dr. Hanzo was FREng, FIET, and a fellow of the EURASIP. In 2009, he received the honorary doctorate Doctor Honoris Causa by the Technical University of Budapest and in 2015 by the University of Edinburgh, U.K. He served as the TPC Chair and the General Chair of the IEEE conferences, presented keynote lectures, and has received a number of distinctions. He is also a Governor of the IEEE VTS. From 2008 to 2012, he was the Editor-in-Chief of the IEEE Press and a Chaired Professor at Tsinghua University, Beijing. He is the Chair in telecommunications with the University of Southampton.